

Rethinking Foundation Models for Medical Image Classification through a Benchmark Study on MedMNIST

Fuping Wu^{1,2} *

FUPING.WU@NDPH.OX.AC.UK

¹ *Nuffield Department of Population Health, University of Oxford, UK*

² *Big Data Institute, University of Oxford, UK*

Bartłomiej W. Papież^{1,2}

Editors: Under Review for MIDL 2025

Abstract

Foundation models are widely employed in medical image analysis, due to their high adaptability and generalizability for downstream tasks. With the increasing number of foundation models being released, model selection has become an important issue. In this work, we study the capabilities of foundation models in medical image classification tasks by conducting a benchmark study on the MedMNIST dataset. Specifically, we adopt various foundation models ranging from convolutional to Transformer-based models and implement both end-to-end training and linear probing for all classification tasks. The results demonstrate the significant potential of these pre-trained models when transferred for medical image classification. We further conduct experiments with different image sizes and various sizes of training data. By analyzing all the results, we provide preliminary, yet useful insights and conclusions on this topic.

Keywords: Foundation model, pre-trained model, medical image, classification, benchmark study.

1. Introduction

Foundation models, which are pre-trained on large-scale diverse datasets, have achieved rapid advancement in various areas, such as computer vision (Awais et al., 2023), natural language processing (Zhou et al., 2023), and audio signal analysis (Huang et al., 2024). These models have been proven effective in adapting to numerous downstream tasks, including semantic segmentation (Wang et al., 2024), recommendation systems (Zhao et al., 2024), showcasing remarkable generalizability and adaptability (Touvron et al., 2023; Anil et al., 2023).

In recent years, the success of foundation models has triggered significant research into their application in medical image analysis (Zhang and Metaxas, 2024), either by transferring models from other fields (Mazurowski et al., 2023) or training models with large-scale medical data (Butoi et al., 2023). While studies have shown the great potential of foundation models in organ segmentation (Ma et al., 2024), clinical reports generation (Thawakar et al.), and medical Q&A systems (Chen et al., 2024), few have conducted large-scale comparisons of the existing models to provide insights into their performance in specific applications (Huix et al., 2024).

In this work, we examine the performance of various foundation models in medical image classification tasks. Although some studies have performed similar comparisons, they

* Corresponding author

were often limited in scope, focusing on small model categories or datasets. For example, [Huix et al. \(2024\)](#) compared eight models across only four medical image classification tasks. [Wang et al. \(2023\)](#) presented a novel dataset with five classification tasks but compared only three models for transfer learning. [Woerner and Baumgartner \(2024\)](#) conducted a benchmark study of few-shot and zero-shot medical image classification with linear probing solely focusing on fine-tuned ResNet-based models. [Baharoon et al. \(2023\)](#) compared DINOv2 ([Oquab et al., 2023](#)) with nine other models on four disease classification tasks.

To provide a comprehensive study of foundation models for medical image classification, we selected a diverse set of models, including four convolutional neural networks (CNN), and eight vision transformer (ViT)-based ([Dosovitskiy, 2020](#)) models. The ViT variants were trained for feature extraction or classification, offering deeper insights into their performance. We used MedMNIST v2 ([Yang et al., 2023](#)), a widely used benchmark for medical image classification, which comprises 12 distinct biomedical 2D datasets. The most relevant work to ours is by [Doerrich et al. \(2024\)](#), who also validated foundation models on MedMNIST v2 but used a different learning pipeline. Notably, compared to ([Doerrich et al., 2024](#)), we adopted more foundation models and achieved significantly better results for eight common models, leading to different conclusions. This finding motivated us to conduct further analyses including the effect of image resizing techniques.

The main contributions of this work are as follows.

- We investigate various foundation models, demonstrating their potential in transferring to medical image classification tasks.
- We study the impact of image size and resizing strategies on the classification performance when transferring these foundation models, as well as their data efficiency.
- We analyze the results and provide several insights for transferring foundation models to medical image classification tasks, such as optimal learning rate settings for different model categories, model selection, and image resizing strategy.

2. Method

2.1. Pre-trained Model Selection

With thousands of pre-trained models publicly available, we select representative backbones for validation and comparison, as shown in Figure 1, ranging from CNN-based to ViT-based architectures. For CNN-based models, we include two baseline models: VGG16 ([Simonyan and Zisserman, 2014](#)) and DenseNet-121 ([Huang et al., 2017](#)), and two models with skip-connection via addition: EfficientNet-B4 ([Tan, 2019](#)) and ResNet-18 ([He et al., 2016](#)). All these CNN-based models were trained with ImageNet-1k ([Russakovsky et al., 2015](#)) for image classification. For ViT-based models, we categorized them into two classes: (1) Four models trained for image classification: Three models, including ViT-B/16 ([Steiner et al., 2021](#)), CLIP ViT-B/16 ([Ilharco et al., 2021](#)) and SAM-C ViT-B/16 ([Chen et al., 2021](#)), are adopted for comparison. These models were trained with different optimization strategies and datasets ([Wightman, 2019](#)), all including ImageNet-1k. We also included SAM ViT-B/16 ([Kirillov et al., 2023](#)) to compare with SAM-C ViT-B/16. Although it was trained with

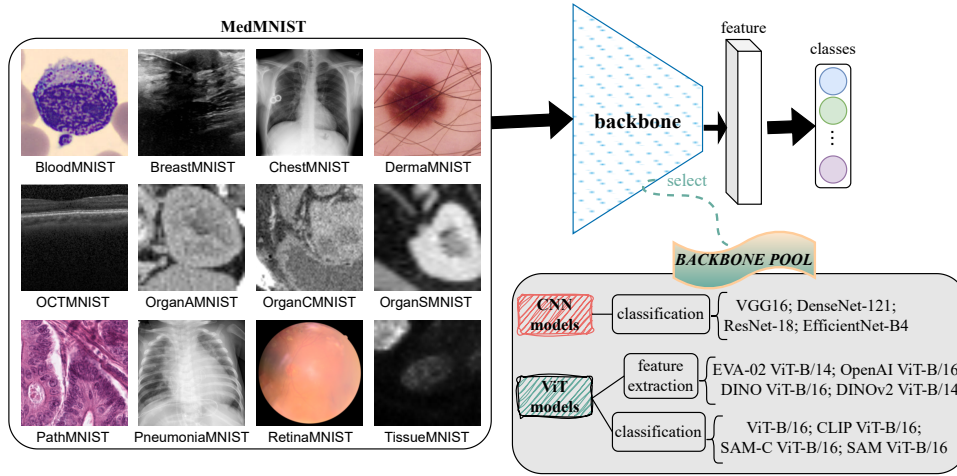


Figure 1: Framework of our study. We evaluate the performance using the MedMNIST dataset collection and select foundation models from a representative pool.

SA-1B ¹ for segmentation, its representations were demonstrated to be useful for various tasks. (2) Four models trained for feature extraction: OpenAI ViT-B/16 (Ilharco et al., 2021) was trained on publicly available image-caption data to maximize the similarity of (*image*, *text*) pairs; EVA-02 ViT-B/14 (Fang et al., 2024) can extract visual representation for reconstructing language-aligned vision features via masked image modeling; DINO ViT-B/16 (Caron et al., 2021) was trained with the self-supervised DINO method, and DINOv2 ViT-B/14 (Oquab et al., 2023) was trained with different losses and a larger dataset, namely LVD-142M. For further details of these models, please refer to Table 3 in Appendix A.

2.2. General Validation Framework

As shown in Figure 1, to validate the selected foundation models on different datasets for classification tasks, we append a one-layer linear classifier after the encoder of each model. For a fair comparison, each classification model is trained with 15,000 iterations, and optimized with the AdamW optimizer (Loshchilov, 2017) using two optimization strategies, linear probing and end-to-end fine-tuning. In linear probing, the encoder is frozen and only the last classifier layer is optimized. The initial learning rate is set to 0.001, which is reduced by 0.9 every 200 iterations. For end-to-end fine-tuning, we adopt the same updating strategy as in linear probing for the classifier, while keeping the learning rate for the encoder, denoted as lr_e , as a constant. Using a low learning rate for the encoder is a common method to adapt the pre-trained model to downstream tasks (Baharoon et al., 2023). The selection of lr_e will be discussed in Section 3.2.

1. <https://segment-anything.com>

3. Benchmark Results

3.1. Datasets

To evaluate the potential of foundation models in medical image classification tasks, we utilize MedMNIST (Yang et al., 2023) collection for validation. As illustrated in Figure 1, MedMNIST comprises 12 2D datasets, with modality spanning X-ray, ultrasound, CT, and electron microscope. Each dataset is available in four different image resolutions: 28×28 , 64×64 , 128×128 , and 224×224 . We primarily use images of 224×224 for testing.

During training, we employ the Cross-Entropy loss for multi-class classification and ordinal regression tasks, and the Binary Cross-Entropy loss for multi-label binary classification problems, such as the multi-label classification task for the ChestMNIST dataset. To maintain consistency with Yang et al. (2023), all experiments are conducted three times on a single NVIDIA A100 GPU. The performance of each model is assessed by the *mean \pm std* of accuracy (ACC) and the area under the receiver operating characteristic curve (AUC).

3.2. Results

3.2.1. LEARNING RATE SELECTION FOR END-TO-END FINE-TUNING STRATEGY

In the end-to-end fine-tuning process, we first determine a suitable learning rate, *i.e.*, lr_e , for the encoder of each foundation model. For the CNN models, we select lr_e from $\{10^{-3}, 10^{-4}, 10^{-5}\}$, while for ViT-based models, we choose from $\{10^{-4}, 10^{-5}, 10^{-6}\}$. Figures 3-14 in Appendix B illustrate the performance of the 12 foundation models across all 12 datasets with various learning rates. Interestingly, the results indicate that for CNN models, $lr_e = 10^{-4}$ generally yields optimal performance, while for ViT-based models, $lr_e = 10^{-5}$ proves to be the best choice in most cases.

3.2.2. END-TO-END FINE-TUNING *vs* LINEAR PROBING

Table 1 and Tables 4-6 in Appendix C present the linear probing and the best end-to-end fine-tuning results for all foundation models across 12 datasets in the MedMNIST collection. Although the 12 models were pre-trained with natural images or languages, they demonstrate significant potential in transfer learning for medical image classification. Notably, end-to-end fine-tuning consistently outperforms linear probing across all datasets, in both accuracy and AUC metrics, except the AUC value on the PathMNIST dataset, where the DINO ViT-B/16 achieves 99.78% AUC with linear probing, 0.03% higher than the former. Particularly, on challenging tasks such as DermaMNIST, OCTMNIST, OrganCMNIST, OrganSMNIST, and TissueMNIST, end-to-end fine-tuning substantially outperforms linear probing.

3.2.3. CNN MODELS *vs* ViT-BASED MODELS

When comparing the results of CNN models with those of ViT-based models, we observe that most of the best performance is achieved by ViT-based models in both linear probing and end-to-end fine-tuning settings. Notably, DenseNet-121 and EfficientNet-B4 achieve the highest accuracy on PneumoniaMNIST and the highest AUC on BloodMNIST, but only under the end-to-end fine-tuning strategy.

Table 1: Results of foundation models on DermaMNIST, PneumoniaMNIST, and BreastMNIST.

Methods	DermaMNIST		PneumoniaMNIST		BreastMNIST	
	ACC	AUC	ACC	AUC	ACC	AUC
END-TO-END						
VGG16	85.49 \pm 0.32	96.17 \pm 0.55	90.12 \pm 0.72	96.78 \pm 1.15	90.60 \pm 1.21	89.88 \pm 1.02
DenseNet-121	87.68 \pm 0.75	96.49 \pm 0.37	94.02\pm0.59	98.13 \pm 0.89	91.24 \pm 0.60	92.18 \pm 0.73
ResNet-18	86.05 \pm 0.78	96.62 \pm 0.32	91.61 \pm 0.79	97.90 \pm 0.35	89.74 \pm 0.91	92.47 \pm 0.66
EfficientNet-B4	88.13 \pm 0.49	97.44 \pm 0.07	90.38 \pm 0.68	97.48 \pm 0.03	87.61 \pm 1.98	90.01 \pm 1.38
ViT-B/16	89.49 \pm 0.24	98.25 \pm 0.16	91.29 \pm 0.72	97.81 \pm 0.98	91.67\pm0.52	94.09\pm0.89
CLIP ViT-B/16	89.64 \pm 0.31	98.31 \pm 0.05	91.29 \pm 0.42	98.80 \pm 0.17	89.53 \pm 1.21	91.02 \pm 1.03
SAM-C ViT-B/16	88.43 \pm 0.07	96.49 \pm 0.41	91.24 \pm 1.45	98.47 \pm 0.16	90.60 \pm 2.47	89.86 \pm 1.34
SAM ViT-B/16	80.62 \pm 0.46	88.53 \pm 1.30	88.25 \pm 1.32	96.44 \pm 0.29	86.75 \pm 0.80	84.06 \pm 0.91
EVA-02 ViT-B/14	88.79 \pm 0.45	94.45 \pm 1.27	90.76 \pm 0.95	97.79 \pm 0.38	87.61 \pm 1.32	88.13 \pm 0.55
OpenAI ViT-B/16	89.74 \pm 0.52	98.08 \pm 0.27	90.01 \pm 0.62	97.90 \pm 0.33	89.96 \pm 1.09	90.78 \pm 0.82
DINO ViT-B/16	89.39 \pm 0.12	98.04 \pm 0.21	91.56 \pm 0.15	97.59 \pm 1.16	88.46 \pm 1.05	91.38 \pm 0.64
DINOv2 ViT-B/14	92.02\pm0.32	98.92\pm0.11	90.81 \pm 0.20	99.24\pm0.14	90.81 \pm 1.68	92.00 \pm 1.99
LINEAR PROBING						
VGG16	76.60 \pm 0.21	92.28 \pm 0.01	86.59 \pm 0.19	97.23 \pm 0.02	84.18 \pm 0.79	88.61 \pm 0.24
DenseNet-121	78.00 \pm 0.34	93.14 \pm 0.03	87.39 \pm 0.45	97.28 \pm 0.01	82.47 \pm 0.79	81.15 \pm 0.27
ResNet-18	74.79 \pm 0.10	90.87 \pm 0.01	85.25 \pm 0.59	95.25 \pm 0.06	81.83 \pm 0.30	81.53 \pm 0.21
EfficientNet-B4	72.38 \pm 0.55	89.28 \pm 0.42	85.52 \pm 0.42	94.10 \pm 0.53	75.42 \pm 1.98	77.40 \pm 1.85
ViT-B/16	83.40 \pm 0.26	96.45 \pm 0.01	88.30 \pm 0.81	97.85 \pm 0.13	89.52\pm0.60	93.74\pm0.17
CLIP ViT-B/16	82.36 \pm 0.16	96.11 \pm 0.05	88.24 \pm 0.15	97.81 \pm 0.04	85.25 \pm 0.52	89.91 \pm 0.19
SAM-C ViT-B/16	83.04 \pm 0.08	96.49 \pm 0.02	89.36 \pm 0.15	98.46 \pm 0.02	87.39 \pm 0.30	92.44 \pm 0.07
SAM ViT-B/16	66.88 \pm 0.00	51.00 \pm 0.53	73.07 \pm 0.26	90.57 \pm 0.04	76.49 \pm 0.30	76.42 \pm 0.02
EVA-02 ViT-B/14	82.70 \pm 0.20	96.09 \pm 0.02	86.21 \pm 0.00	96.82 \pm 0.02	87.82 \pm 0.00	90.84 \pm 0.05
OpenAI ViT-B/16	82.80 \pm 0.23	96.14 \pm 0.04	86.91 \pm 0.15	96.75 \pm 0.00	86.75 \pm 0.30	90.64 \pm 0.28
DINO ViT-B/16	84.87\pm0.36	97.06\pm0.02	92.41\pm0.42	98.87\pm0.03	88.24 \pm 0.30	92.73 \pm 0.07
DINOv2 ViT-B/14	83.97 \pm 0.08	96.62 \pm 0.02	90.65 \pm 0.65	98.41 \pm 0.08	87.39 \pm 1.08	92.50 \pm 0.04
Results from Zhang et al. (2024) for models pre-trained on medical data						
BiomedGPT	86.6	-	-	-	79.5	-
BiomedCLIP	71.9	-	-	-	82.2	-
MedSAM	72.3	-	-	-	76.9	-

Among ViT-based methods, ViT-B/16 generally excels in the category of classification-targeted pre-trained models. For feature extraction models, DINO or DINOv2 frequently delivers the best results. Interestingly, SAM-C ViT-B/16 consistently outperforms SAM ViT-B/16 across all classification tasks, especially with the linear probing strategy. This may be attributed to SAM being primarily trained for segmentation tasks, which could hinder its ability to capture global information effectively for classification purposes.

3.2.4. IMPACT OF TRAINING PIPELINE

It is important to note that [Doerrich et al. \(2024\)](#) adopted a different training pipeline when validating foundation models on MedMNIST, which led to conclusions that diverged from ours. Specifically, they employed the AdamW optimizer with a learning rate of 0.0001 and a cosine annealing learning rate scheduler ([Loshchilov and Hutter, 2022](#)) with a single cycle. When comparing the results for the 8 common models, highlighted in Table 3 in Appendix A, we found similar outcomes under the linear probing strategy. However, our results surpass theirs in the end-to-end fine-tuning setting, especially for ViT-based models. For instance, on BreastMNIST, ViT-B/16 achieved an accuracy of 83.76 ± 1.09 and an AUC of 86.18 ± 0.26 in their setup. In contrast, our setup yielded better results, with an accuracy of 91.67 ± 0.52 and an AUC of 94.09 ± 0.89 . Similarly, on DermaMNIST, DINO ViT-B/16 achieved an accuracy of 81.31 ± 1.05 in their work *vs* 89.39 ± 0.12 in ours.

Based on a different training pipeline, [Doerrich et al. \(2024\)](#) delivered several conclusions that could be contradictory to the results in this work. For example, they concluded that self-supervised pretraining models, such as CLIP and DINO, do not always improve medical image classification results in end-to-end fine-tuning while demonstrating enhanced performance with linear probing. Conversely, our results demonstrate that these models not only improve the performance in end-to-end fine-tuning, but also outperform linear probing. Additionally, they concluded that CNN models consistently outperform ViT-based models in accuracy with end-to-end training, while in our work we have an almost opposite conclusion. For example, on the DermaMNIST dataset, DINOv2 ViT-B/14, reached the highest accuracy of 92.02 ± 0.32 , while the best-performing CNN model, EfficientNet-B4, obtained an accuracy of 88.13 ± 0.49 .

4. Discussion

4.1. Effect of Image Size and Resizing Strategy

We further investigated the impact of resizing strategies on performance, particularly when handling smaller image sizes, as many foundation models require a fixed input size. Specifically, we compare zero-padding and scaling strategies for both end-to-end fine-tuning and linear probing, focusing on the DermaMNIST dataset with image sizes of 28×28 , 64×64 and 128×128 . Table 2 and Table 7 in Appendix D present the results with scaling and zero-padding strategies, respectively. The findings reveal that, generally, accuracy improves with larger image sizes when using zero-padding. Similarly, for the scaling strategy, larger image sizes typically result in higher accuracy. However, the differences, particularly among sizes of 64×64 , 128×128 , and 224×224 are marginal. Comparison plots illustrating these trends can be found in Figures 15-18 in Appendix E. Notably, for end-to-end fine-tuning, scaling tends to yield better accuracy than zero-padding across all image sizes. Conversely, for linear probing, the performance gap between scaling and zero-padding narrows, particularly when the image size is 128×128 . For a detailed comparison, please refer to Figures 19-24 in Appendix E.

Table 2: Results of foundation models on DermaMNIST of different image sizes using scaling to resize the original images into a resolution of 224×224 .

Methods	28×28		64×64		128×128	
	ACC	AUC	ACC	AUC	ACC	AUC
END-TO-END						
VGG16	77.36 \pm 0.32	91.76 \pm 0.40	83.62 \pm 0.20	95.91 \pm 0.28	85.35 \pm 0.80	96.10 \pm 0.23
DenseNet-121	78.04 \pm 0.51	90.29 \pm 1.03	85.15 \pm 0.08	95.51 \pm 0.47	86.57 \pm 0.65	96.43 \pm 0.50
ResNet-18	79.83 \pm 0.58	92.98 \pm 0.28	84.80 \pm 1.09	95.74 \pm 0.44	85.80 \pm 0.68	96.46 \pm 0.38
EfficientNet-B4	76.31 \pm 1.11	91.37 \pm 0.46	84.42 \pm 0.80	95.66 \pm 0.43	86.37 \pm 0.94	96.75 \pm 0.31
ViT-B/16	81.68 \pm 0.96	95.00 \pm 0.21	87.65 \pm 0.21	97.80 \pm 0.24	88.66 \pm 0.10	98.02 \pm 0.15
CLIP ViT-B/16	81.60 \pm 0.40	94.63 \pm 0.15	87.96 \pm 0.60	97.67 \pm 0.10	89.21 \pm 0.16	98.13 \pm 0.04
SAM-C ViT-B/16	81.55 \pm 0.32	92.87 \pm 0.82	87.25 \pm 0.38	96.45 \pm 0.17	87.48 \pm 0.84	96.89 \pm 0.10
SAM ViT-B/16	77.01 \pm 1.21	86.51 \pm 1.44	80.02 \pm 0.33	88.23 \pm 1.35	79.98 \pm 1.14	87.89 \pm 0.41
EVA-02 ViT-B/14	80.35 \pm 0.36	84.75 \pm 0.57	86.78 \pm 0.41	92.26 \pm 0.71	87.65 \pm 0.44	92.63 \pm 0.67
OpenAI ViT-B/16	81.31 \pm 0.24	94.43 \pm 0.30	88.26 \pm 0.72	97.94 \pm 0.18	89.33 \pm 0.12	98.00 \pm 0.05
DINO ViT-B/16	80.53 \pm 0.40	94.16 \pm 0.45	86.75 \pm 0.28	97.47 \pm 0.13	88.10 \pm 0.45	97.72 \pm 0.06
DINOv2 ViT-B/14	82.19\pm0.25	95.30\pm0.10	89.83\pm0.25	98.41\pm0.10	91.19\pm0.48	98.63\pm0.01
LINEAR PROBING						
VGG16	74.96 \pm 0.11	90.67 \pm 0.03	77.04 \pm 0.29	92.38 \pm 0.02	76.48 \pm 0.37	92.49 \pm 0.12
DenseNet-121	73.23 \pm 0.16	90.69 \pm 0.14	77.04 \pm 0.43	92.66 \pm 0.05	76.94 \pm 0.29	93.01 \pm 0.05
ResNet-18	73.18 \pm 0.13	87.69 \pm 0.07	75.01 \pm 0.50	90.73 \pm 0.11	75.10 \pm 0.06	91.47 \pm 0.06
EfficientNet-B4	69.38 \pm 0.46	84.40 \pm 0.65	72.85 \pm 0.51	88.64 \pm 0.20	72.40 \pm 0.55	88.91 \pm 0.59
ViT-B/16	77.27 \pm 0.35	93.23 \pm 0.05	81.23 \pm 0.29	95.36 \pm 0.08	82.61 \pm 0.52	96.12 \pm 0.16
CLIP ViT-B/16	75.11 \pm 0.22	92.84 \pm 0.12	79.87 \pm 0.22	94.81 \pm 0.04	80.76 \pm 0.19	95.45 \pm 0.05
SAM-C ViT-B/16	77.37 \pm 0.23	93.92 \pm 0.09	80.63 \pm 0.72	95.63 \pm 0.23	81.58 \pm 0.25	96.10 \pm 0.06
SAM ViT-B/16	66.88 \pm 0.00	43.72 \pm 0.24	66.88 \pm 0.00	45.91 \pm 0.34	66.88 \pm 0.00	49.15 \pm 0.54
EVA-02 ViT-B/14	78.09 \pm 0.02	94.13\pm0.01	82.76 \pm 0.13	96.12 \pm 0.00	82.34 \pm 0.18	95.82 \pm 0.03
OpenAI ViT-B/16	76.77 \pm 0.25	93.03 \pm 0.09	80.07 \pm 0.19	95.19 \pm 0.01	82.59 \pm 0.16	95.81 \pm 0.01
DINO ViT-B/16	78.30\pm0.41	93.47 \pm 0.03	82.78\pm0.12	96.20\pm0.04	84.56\pm0.26	96.79\pm0.01
DINOv2 ViT-B/14	75.56 \pm 0.27	91.75 \pm 0.08	80.45 \pm 0.25	94.98 \pm 0.02	82.61 \pm 0.34	96.09 \pm 0.08

4.2. Data Efficiency

We further investigated whether these foundation models can be adapted to medical image classification tasks with limited training data using end-to-end fine-tuning or linear probing. This analysis was conducted on the DermaMNIST dataset, varying the number of training images per class in $\{20, 40, 60, 80, 100, 200, 400, 600\}$. As illustrated in Figure 2, the accuracy of DINO ViT-B/16 improves significantly with an increasing number of training images for both end-to-end fine-tuning and linear probing. This indicates the low data efficiency of DINO ViT-B/16 when transferring to this task. Similar trends were observed across the other 11 models as detailed in Figures 25-34 in Appendix F. These findings suggest that few-shot learning for foundation model transferring remains challenging, and requires delicate optimization strategies.

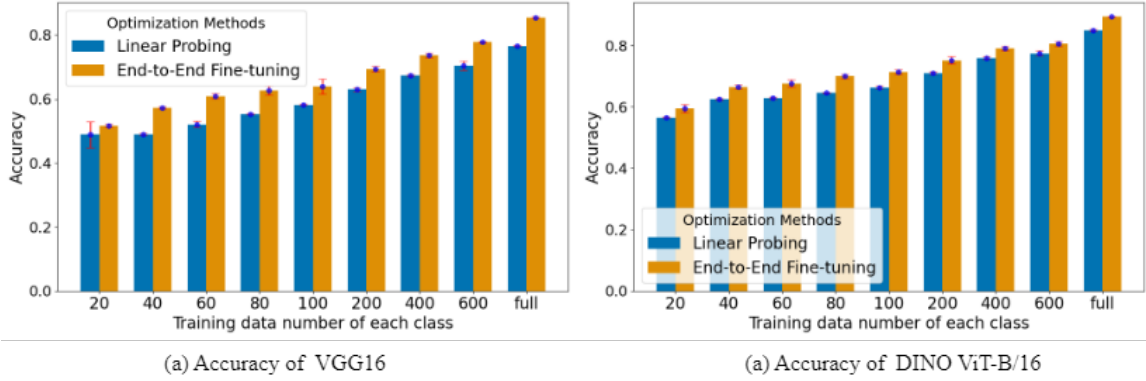


Figure 2: Accuracy of DINO ViT-B/16 on DermaMNIST with various numbers of training data for each class, and “full” means using all training data.

4.3. Transferring Foundation Models Pre-trained on Medical Data

Zhang et al. (2024) fine-tuned three foundation models pre-trained on medical data, including BioMedGPT (Zhang et al., 2024), BioMedCLIP (Zhang et al., 2023) and MedSAM (Ma et al., 2024), on seven datasets from the MedMNIST collection. Their results, presented at the bottom of Table 1 and Tables 4-6 in Appendix C are generally poorer compared to the models we adopted. This suggests the need for further development of foundation models based on medical data. However, the absence of linear probing results for these models limits the completeness of the comparison, which we propose to address in future work.

5. Conclusion

In this work, we evaluated the performance of foundation models on medical image classification tasks, selecting 12 representative models spanning CNN and ViT-based models. We employed both end-to-end fine-tuning and linear probing strategies for model transfer. Our results demonstrate the significant potential of foundation models in these tasks. Additionally, we explored the impact of image size and resizing strategies, deriving useful insights from our findings. Despite these promising results, several limitations remain: (1) Our validation is limited to the MedMNIST collection. Including additional datasets would provide more comprehensive conclusions; (2) Our analysis of resizing strategies is limited to the DermaMNIST dataset. A broader validation across all 12 datasets in the collection is planned for future work. (3) The current analysis lacks depth, particularly regarding model performance on specific classes within each task. A more detailed discussion will be provided. (4) The biases of each model across different medical image classification tasks are yet to be understood (Alloula et al., 2024).

Acknowledgments

The authors would like to acknowledge the funding from Novo Nordisk to support this work.

References

- Anissa Alloula, Rima Mustafa, Daniel R McGowan, and Bartłomiej W Papież. On biases in a UK Biobank-based retinal image classification model. In *MICCAI Workshop on Fairness of AI in Medical Imaging*, pages 140–150. Springer, 2024.
- Rohan Anil, Andrew M Dai, Orhan Firat, Melvin Johnson, Dmitry Lepikhin, Alexandre Passos, Siamak Shakeri, Emanuel Taropa, Paige Bailey, Zhifeng Chen, et al. Palm 2 technical report. *arXiv preprint arXiv:2305.10403*, 2023.
- Muhammad Awais, Muzammal Naseer, Salman Khan, Rao Muhammad Anwer, Hisham Cholakkal, Mubarak Shah, Ming-Hsuan Yang, and Fahad Shahbaz Khan. Foundational models defining a new era in vision: A survey and outlook. *arXiv preprint arXiv:2307.13721*, 2023.
- Mohammed Baharoon, Waseem Qureshi, Jiahong Ouyang, Yanwu Xu, Kilian Phol, Abdulrhman Aljouie, and Wei Peng. Towards general purpose vision foundation models for medical image analysis: An experimental study of dinov2 on radiology benchmarks. *arXiv preprint arXiv:2312.02366*, 2023.
- Victor Ion Butoi, Jose Javier Gonzalez Ortiz, Tianyu Ma, Mert R Sabuncu, John Guttag, and Adrian V Dalca. Universeg: Universal medical image segmentation. In *Proceedings of the IEEE/CVF International Conference on Computer Vision*, pages 21438–21451, 2023.
- Mathilde Caron, Hugo Touvron, Ishan Misra, Herv'e J'egou, Julien Mairal, Piotr Bojanowski, and Armand Joulin. Emerging properties in self-supervised vision transformers. In *Proceedings of the IEEE/CVF international conference on computer vision*, pages 9650–9660, 2021.
- Xiangning Chen, Cho-Jui Hsieh, and Boqing Gong. When vision transformers outperform resnets without pre-training or strong data augmentations. *arXiv preprint arXiv:2106.01548*, 2021.
- Zhihong Chen, Maya Varma, Jean-Benoit Delbrouck, Magdalini Paschali, Louis Blanke-meier, Dave Van Veen, Jeya Maria Jose Valanarasu, Alaa Youssef, Joseph Paul Cohen, Eduardo Pontes Reis, et al. Chexagent: Towards a foundation model for chest x-ray interpretation. *arXiv preprint arXiv:2401.12208*, 2024.
- Sebastian Doerrich, Francesco Di Salvo, Julius Brockmann, and Christian Ledig. Rethinking model prototyping through the medmnist+ dataset collection. *arXiv preprint arXiv:2404.15786*, 2024.
- Alexey Dosovitskiy. An image is worth 16x16 words: Transformers for image recognition at scale. *arXiv preprint arXiv:2010.11929*, 2020.

- Yuxin Fang, Quan Sun, Xinggang Wang, Tiejun Huang, Xinlong Wang, and Yue Cao. Eva-02: A visual representation for neon genesis. *Image and Vision Computing*, 149:105171, 2024.
- Kaiming He, Xiangyu Zhang, Shaoqing Ren, and Jian Sun. Deep residual learning for image recognition. In *Proceedings of the IEEE conference on computer vision and pattern recognition*, pages 770–778, 2016.
- Gao Huang, Zhuang Liu, Laurens Van Der Maaten, and Kilian Q Weinberger. Densely connected convolutional networks. In *Proceedings of the IEEE conference on computer vision and pattern recognition*, pages 4700–4708, 2017.
- Rongjie Huang, Mingze Li, Dongchao Yang, Jiatong Shi, Xuankai Chang, Zhenhui Ye, Yuning Wu, Zhiqing Hong, Jiawei Huang, Jinglin Liu, et al. Audiogpt: Understanding and generating speech, music, sound, and talking head. In *Proceedings of the AAAI Conference on Artificial Intelligence*, volume 38, pages 23802–23804, 2024.
- Joana Palés Huix, Adithya Raju Ganeshan, Johan Fredin Haslum, Magnus Söderberg, Christos Matsoukas, and Kevin Smith. Are natural domain foundation models useful for medical image classification? In *Proceedings of the IEEE/CVF Winter Conference on Applications of Computer Vision*, pages 7634–7643, 2024.
- Gabriel Ilharco, Mitchell Wortsman, Ross Wightman, Cade Gordon, Nicholas Carlini, Rohan Taori, Achal Dave, Vaishaal Shankar, Hongseok Namkoong, John Miller, Hananeh Hajishirzi, Ali Farhadi, and Ludwig Schmidt. Openclip, July 2021. URL <https://doi.org/10.5281/zenodo.5143773>. If you use this software, please cite it as below.
- Alexander Kirillov, Eric Mintun, Nikhila Ravi, Hanzi Mao, Chloe Rolland, Laura Gustafson, Tete Xiao, Spencer Whitehead, Alexander C Berg, Wan-Yen Lo, et al. Segment anything. In *Proceedings of the IEEE/CVF International Conference on Computer Vision*, pages 4015–4026, 2023.
- I Loshchilov. Decoupled weight decay regularization. *arXiv preprint arXiv:1711.05101*, 2017.
- Ilya Loshchilov and Frank Hutter. Sgdr: Stochastic gradient descent with warm restarts. In *International Conference on Learning Representations*, pages 1–13, 2022.
- Jun Ma, Yuting He, Feifei Li, Lin Han, Chenyu You, and Bo Wang. Segment anything in medical images. *Nature Communications*, 15:654, 2024.
- Maciej A Mazurowski, Haoyu Dong, Hanxue Gu, Jichen Yang, Nicholas Konz, and Yixin Zhang. Segment anything model for medical image analysis: an experimental study. *Medical Image Analysis*, 89:102918, 2023.
- Maxime Oquab, Timothée Darcet, Théo Moutakanni, Huy Vo, Marc Szafraniec, Vasil Khalidov, Pierre Fernandez, Daniel Haziza, Francisco Massa, Alaaeldin El-Nouby, et al. Dinov2: Learning robust visual features without supervision. *arXiv preprint arXiv:2304.07193*, 2023.

- Olga Russakovsky, Jia Deng, Hao Su, Jonathan Krause, Sanjeev Satheesh, Sean Ma, Zhiheng Huang, Andrej Karpathy, Aditya Khosla, Michael Bernstein, et al. Imagenet large scale visual recognition challenge. *International journal of computer vision*, 115:211–252, 2015.
- Karen Simonyan and Andrew Zisserman. Very deep convolutional networks for large-scale image recognition. *arXiv preprint arXiv:1409.1556*, 2014.
- Andreas Steiner, Alexander Kolesnikov, Xiaohua Zhai, Ross Wightman, Jakob Uszkoreit, and Lucas Beyer. How to train your vit? data, augmentation, and regularization in vision transformers. *arXiv preprint arXiv:2106.10270*, 2021.
- Mingxing Tan. Efficientnet: Rethinking model scaling for convolutional neural networks. *arXiv preprint arXiv:1905.11946*, pages 6105–6114, 2019.
- Omkar Chakradhar Thawakar, Abdelrahman M Shaker, Sahal Shaji Mullappilly, Hisham Cholakkal, Rao Muhammad Anwer, Salman Khan, Jorma Laaksonen, and Fahad Khan. Xraygpt: Chest radiographs summarization using large medical vision-language models. In *Proceedings of the 23rd Workshop on Biomedical Natural Language Processing*, pages 440–448.
- Hugo Touvron, Thibaut Lavril, Gautier Izacard, Xavier Martinet, Marie-Anne Lachaux, Timothée Lacroix, Baptiste Rozière, Naman Goyal, Eric Hambro, Faisal Azhar, et al. Llama: Open and efficient foundation language models. *arXiv preprint arXiv:2302.13971*, 2023.
- Dequan Wang, Xiaosong Wang, Lilong Wang, Mengzhang Li, Qian Da, Xiaoqiang Liu, Xiangyu Gao, Jun Shen, Junjun He, Tian Shen, et al. A real-world dataset and benchmark for foundation model adaptation in medical image classification. *Scientific Data*, 10(1): 574, 2023.
- Wenhai Wang, Zhe Chen, Xiaokang Chen, Jiannan Wu, Xizhou Zhu, Gang Zeng, Ping Luo, Tong Lu, Jie Zhou, Yu Qiao, et al. Visionllm: Large language model is also an open-ended decoder for vision-centric tasks. *Advances in Neural Information Processing Systems*, 36, 2024.
- Ross Wightman. Pytorch image models. <https://github.com/huggingface/pytorch-image-models>, 2019.
- Stefano Woerner and Christian F Baumgartner. Navigating data scarcity using foundation models: A benchmark of few-shot and zero-shot learning approaches in medical imaging. In *International Workshop on Foundation Models for General Medical AI*, pages 30–39. Springer, 2024.
- Jiancheng Yang, Rui Shi, Donglai Wei, Zequan Liu, Lin Zhao, Bilian Ke, Hanspeter Pfister, and Bingbing Ni. Medmnist v2-a large-scale lightweight benchmark for 2d and 3d biomedical image classification. *Scientific Data*, 10(1):41, 2023.

- Kai Zhang, Rong Zhou, Eashan Adhikarla, Zhiling Yan, Yixin Liu, Jun Yu, Zhengliang Liu, Xun Chen, Brian D Davison, Hui Ren, et al. A generalist vision–language foundation model for diverse biomedical tasks. *Nature Medicine*, pages 1–13, 2024.
- Shaoting Zhang and Dimitris Metaxas. On the challenges and perspectives of foundation models for medical image analysis. *Medical image analysis*, 91:102996, 2024.
- Sheng Zhang, Yanbo Xu, Naoto Usuyama, Hanwen Xu, Jaspreet Bagga, Robert Tinn, Sam Preston, Rajesh Rao, Mu Wei, Naveen Valluri, et al. Biomedclip: a multimodal biomedical foundation model pretrained from fifteen million scientific image-text pairs. *arXiv preprint arXiv:2303.00915*, 2023.
- Zihuai Zhao, Wenqi Fan, Jiatong Li, Yunqing Liu, Xiaowei Mei, Yiqi Wang, Zhen Wen, Fei Wang, Xiangyu Zhao, Jiliang Tang, et al. Recommender systems in the era of large language models (llms). *IEEE Transactions on Knowledge and Data Engineering*, 2024.
- Ce Zhou, Qian Li, Chen Li, Jun Yu, Yixin Liu, Guangjing Wang, Kai Zhang, Cheng Ji, Qiben Yan, Lifang He, et al. A comprehensive survey on pretrained foundation models: A history from bert to chatgpt. *arXiv preprint arXiv:2302.09419*, 2023.

Appendix A. Details of the Evaluated Models.

Table 3: Details of the 12 evaluated models. ‘✓’ means the model was also validated in the work of Doerrich et al. (2024).

Model	Params (M)	Model Task	Training Data	Source
CNN-based Models				
VGG16 (✓)	138.4	Image classification	ImageNet-1k	timm ² with identifier: <i>vgg16.tv_in1k</i>
ResNet-18 (✓)	11.7	Image classification	ImageNet-1k	timm with identifier: <i>resnet18.a1_in1k</i>
DenseNet121 (✓)	8.0	Image classification	ImageNet-1k	timm with identifier: <i>densenet121.ra_in1k</i>
EfficientNet-B4 (✓)	19.3	Image classification	ImageNet-1k	timm with identifier: <i>efficientnet_b4.ra2_in1k</i>
Transformer-based Models				
ViT-B/16 (✓)	86.6	Image classification	ImageNet-21k, ImageNet-1k	timm with identifier: <i>vit_base_patch16_224.augreg2_in21k_ft_in1k</i>
CLIP ViT-B/16 (✓)	86.6	Image classification	LAION-2B, ImageNet-12k, ImageNet-1k	timm with identifier: <i>vit_base_patch16_clip_224.laion2b_ft_in12k_in1k</i>
SAM-C ViT-B/16	86.6	Image classification	ImageNet-1k	timm with identifier: <i>vit_base_patch16_224.sam_in1k</i>
SAM ViT-B/16 (✓)	89.7	Image segmentation	SA-1B	timm with identifier: <i>samvit_base_patch16.sa1b</i>
EVA-02 ViT-B/14	85.8	Feature extraction	ImageNet-22k	timm with identifier: <i>eva02_base_patch14_224.mim_in22k</i>
OpenAI ViT-B/16	86.6	Feature extraction	Image-text open source	timm with identifier: <i>vit_base_patch16_clip_224.openai</i>
DINO ViT-B/16 (✓)	85.8	Feature extraction	ImageNet-1k	timm with identifier: <i>vit_base_patch16_224.dino</i>
DINOv2 ViT-B/14	86.6	Feature extraction	LVD-142M	timm with identifier: <i>vit_base_patch14_dinov2.lvd142m</i>
MedSAM ViT-B/16	89.7	Image segmentation	ImageNet-1k, Medical image open source	Github repository ³

2. timm at Huggingface: <https://huggingface.co/timm>

3. <https://github.com/bowang-lab/MedSAM>

Appendix B. Tuning Learning Rate for Foundation Models

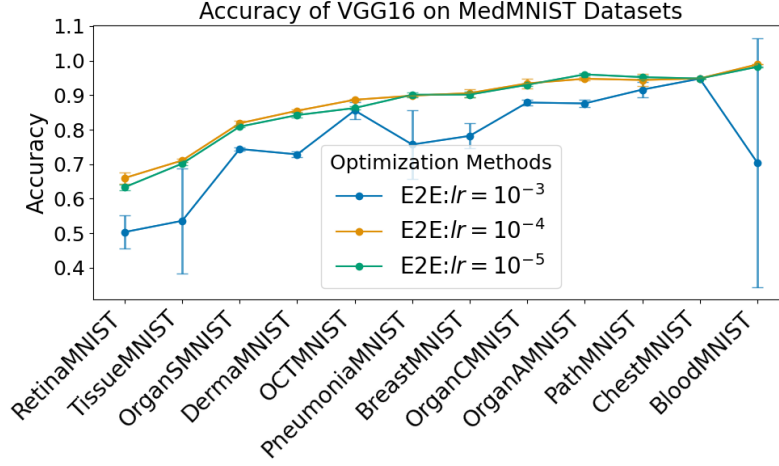


Figure 3: Comparing the Accuracy of VGG16 with the learning rate of the encoder ranging in $\{10^{-3}, 10^{-4}, 10^{-5}\}$ on different datasets.

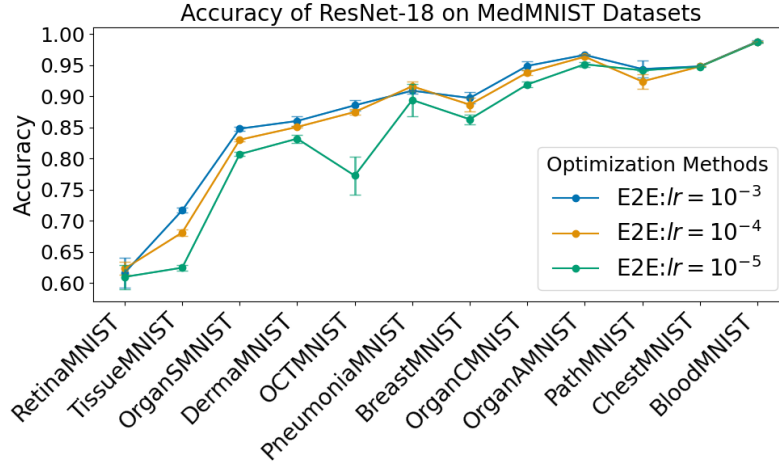


Figure 4: Comparing the Accuracy of ResNet-18 with the learning rate of the encoder ranging in $\{10^{-3}, 10^{-4}, 10^{-5}\}$ on different datasets.

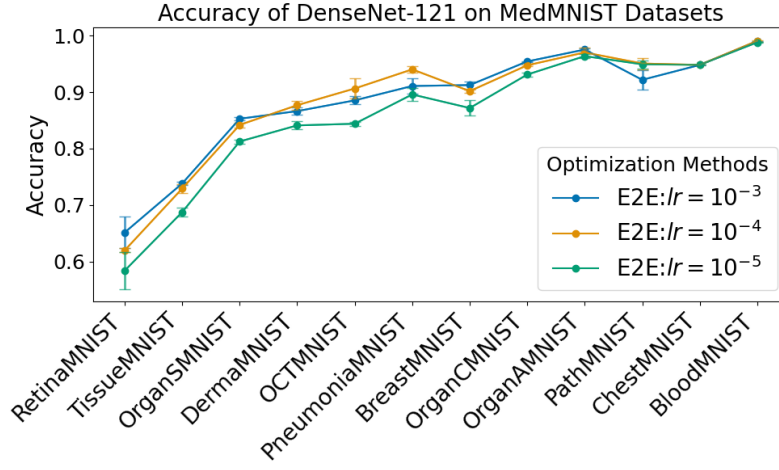


Figure 5: Comparing the Accuracy of DenseNet-121 with the learning rate of the encoder ranging in $\{10^{-3}, 10^{-4}, 10^{-5}\}$ on different datasets.

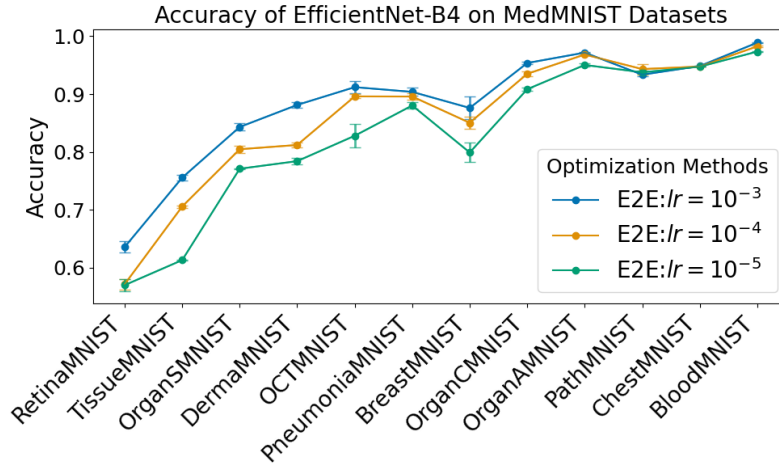


Figure 6: Comparing the Accuracy of EfficientNet-B4 with the learning rate of the encoder ranging in $\{10^{-3}, 10^{-4}, 10^{-5}\}$ on different datasets.

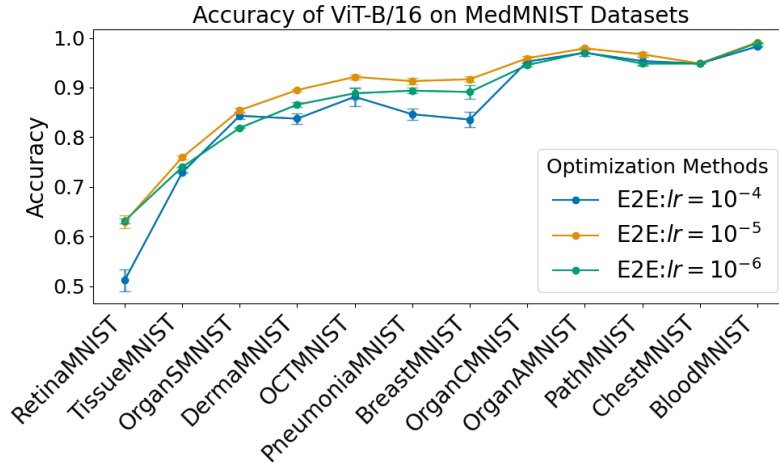


Figure 7: Tuning the learning rate for the encoder of ViT-B/16 ranging in $\{10^{-4}, 10^{-5}, 10^{-6}\}$ on different datasets.

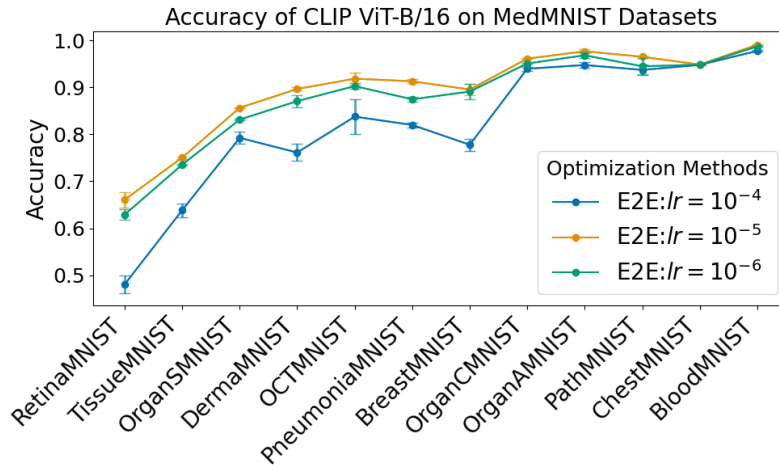


Figure 8: Comparing the Accuracy of CLIP ViT-B/16 with the learning rate of the encoder ranging in $\{10^{-4}, 10^{-5}, 10^{-6}\}$ on different datasets.

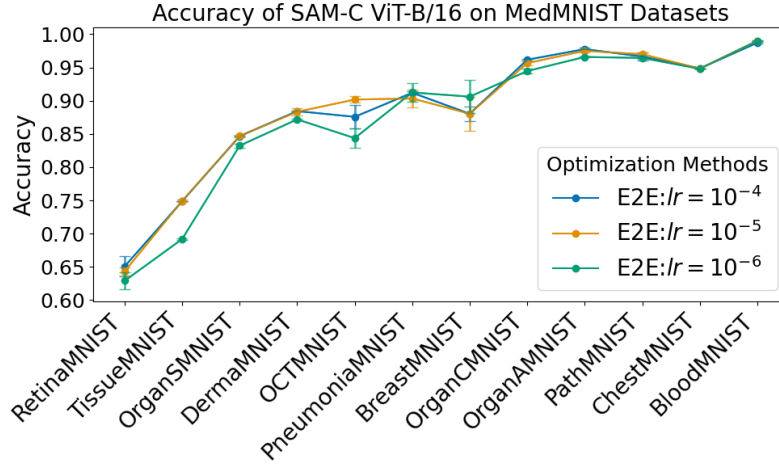


Figure 9: Comparing the Accuracy of RSAM-C ViT-B/16 with the learning rate of the encoder ranging in $\{10^{-4}, 10^{-5}, 10^{-6}\}$ on different datasets.

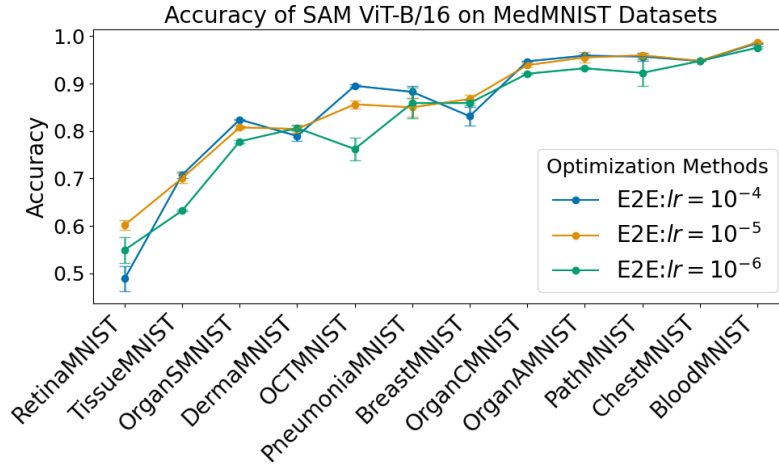


Figure 10: Comparing the Accuracy of SAM ViT-B/16 with the learning rate of the encoder ranging in $\{10^{-4}, 10^{-5}, 10^{-6}\}$ on different datasets.

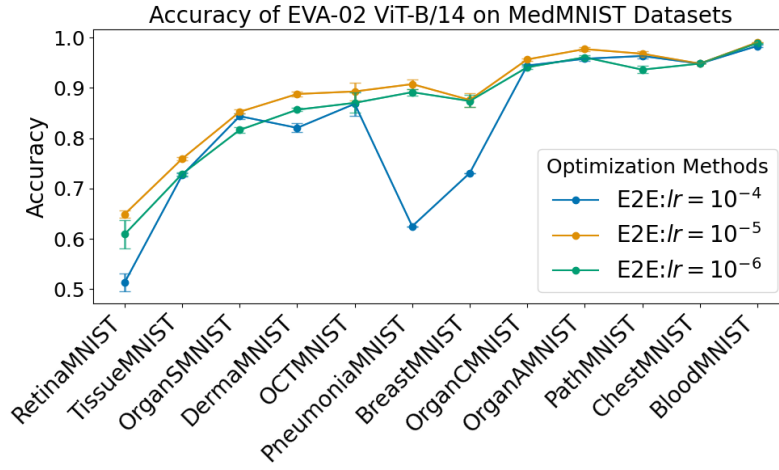


Figure 11: Comparing the Accuracy of EVA-02 ViT-B/14 with the learning rate of the encoder ranging in $\{10^{-4}, 10^{-5}, 10^{-6}\}$ on different datasets.

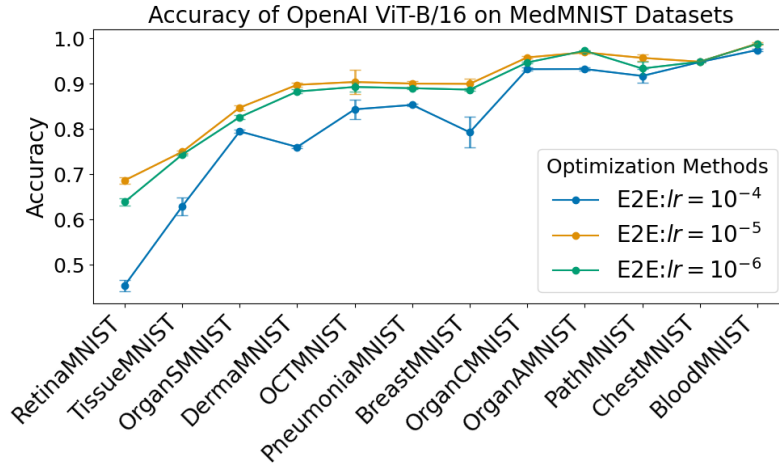


Figure 12: Comparing the Accuracy of OpenAI ViT-B/16 with the learning rate of the encoder ranging in $\{10^{-4}, 10^{-5}, 10^{-6}\}$ on different datasets.

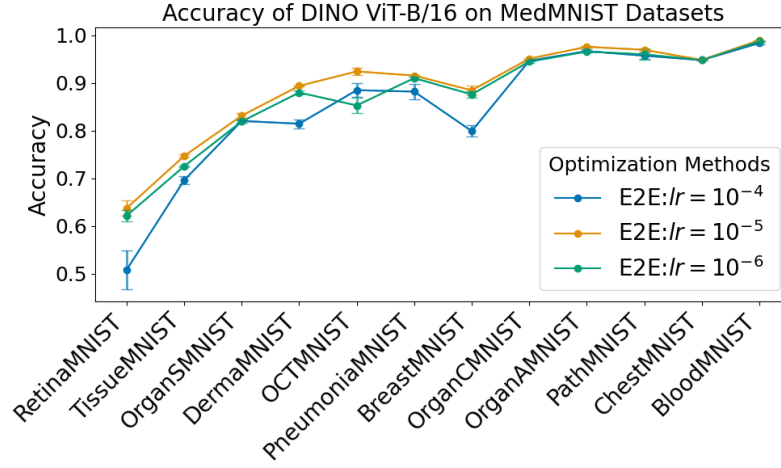


Figure 13: Comparing the Accuracy of DINO ViT-B/16 with the learning rate of the encoder ranging in $\{10^{-4}, 10^{-5}, 10^{-6}\}$ on different datasets.

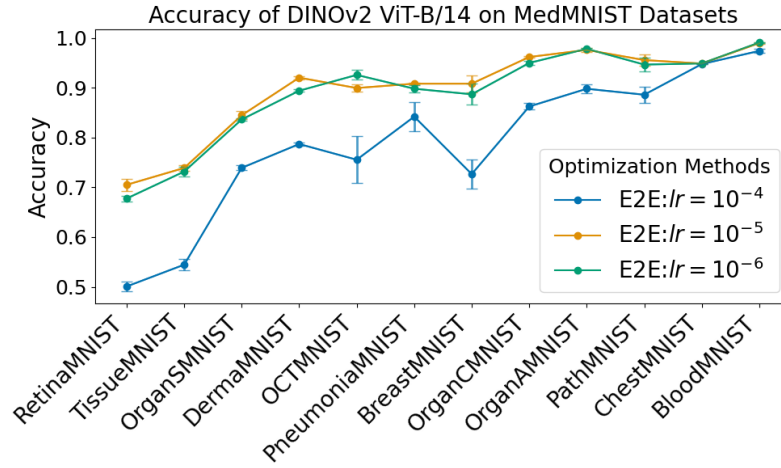


Figure 14: Comparing the Accuracy of DINOv2 ViT-B/14 with the learning rate of the encoder ranging in $\{10^{-4}, 10^{-5}, 10^{-6}\}$ on different datasets.

Appendix C. Results of Foundation Models on MedMNIST

Table 4: Results of foundation models on BloodMNIST, ChestMNIST, and OCTMNIST.

Methods	BloodMNIST		ChestMNIST		OCTMNIST	
	ACC	AUC	ACC	AUC	ACC	AUC
END-TO-END						
VGG16	98.90 \pm 0.04	99.94 \pm 0.01	94.84 \pm 0.02	80.18 \pm 0.97	88.67 \pm 0.34	98.69 \pm 0.22
DenseNet-121	99.06 \pm 0.13	99.93 \pm 0.00	94.81 \pm 0.01	70.75 \pm 0.84	90.63 \pm 1.76	99.27 \pm 0.30
ResNet-18	98.81 \pm 0.23	99.93 \pm 0.00	94.82 \pm 0.03	80.13 \pm 0.98	88.57 \pm 0.90	99.01 \pm 0.08
EfficientNet-B4	98.89 \pm 0.10	99.95\pm0.00	94.84 \pm 0.00	82.65 \pm 0.07	91.20 \pm 0.99	99.36 \pm 0.28
ViT-B/16	99.11\pm0.04	99.95 \pm 0.01	94.85 \pm 0.01	81.28 \pm 0.91	92.13 \pm 0.46	99.63 \pm 0.09
CLIP ViT-B/16	99.06 \pm 0.13	99.95 \pm 0.01	94.84 \pm 0.00	81.67 \pm 0.91	91.83 \pm 1.36	99.55 \pm 0.10
SAM-C ViT-B/16	99.01 \pm 0.10	99.91 \pm 0.03	94.84 \pm 0.01	71.17 \pm 1.47	90.17 \pm 0.46	99.22 \pm 0.14
SAM ViT-B/16	98.69 \pm 0.06	99.70 \pm 0.07	94.79 \pm 0.00	62.25 \pm 1.00	89.53 \pm 0.26	99.10 \pm 0.38
EVA-02 ViT-B/14	99.05 \pm 0.06	99.68 \pm 0.10	94.83 \pm 0.01	67.06 \pm 0.90	89.30 \pm 1.73	98.32 \pm 0.82
OpenAI ViT-B/16	98.83 \pm 0.33	99.95 \pm 0.01	94.84 \pm 0.03	76.18 \pm 1.67	90.37 \pm 2.64	99.54 \pm 0.29
DINO ViT-B/16	98.97 \pm 0.04	99.95 \pm 0.01	94.83 \pm 0.03	80.83 \pm 0.28	92.43 \pm 0.79	99.53 \pm 0.13
DINOv2 ViT-B/14	99.06 \pm 0.10	99.94 \pm 0.00	94.87\pm0.01	83.22\pm0.48	92.57\pm0.99	99.80\pm0.02
LINEAR PROBING						
VGG16	91.87 \pm 0.08	99.42 \pm 0.00	94.75 \pm 0.00	73.63 \pm 0.14	68.63 \pm 0.25	96.20 \pm 0.04
DenseNet-121	95.95 \pm 0.06	99.82 \pm 0.00	94.75 \pm 0.00	72.39 \pm 0.87	62.83 \pm 0.21	95.00 \pm 0.06
ResNet-18	92.84 \pm 0.05	99.46 \pm 0.01	94.74 \pm 0.00	68.57 \pm 0.01	55.43 \pm 0.17	91.52 \pm 0.13
EfficientNet-B4	91.71 \pm 0.33	99.35 \pm 0.01	94.70 \pm 0.01	66.39 \pm 0.27	63.27 \pm 1.24	91.95 \pm 0.33
ViT-B/16	98.12 \pm 0.06	99.93 \pm 0.00	94.73 \pm 0.00	74.61 \pm 0.61	81.40 \pm 0.28	98.82 \pm 0.01
CLIP ViT-B/16	96.45 \pm 0.08	99.88 \pm 0.00	94.75 \pm 0.00	75.67 \pm 0.06	79.67 \pm 0.61	98.64 \pm 0.01
SAM-C ViT-B/16	97.14 \pm 0.19	99.89 \pm 0.01	94.76\pm0.01	75.86 \pm 0.03	75.47 \pm 0.17	98.87 \pm 0.01
SAM ViT-B/16	56.94 \pm 0.10	91.17 \pm 0.02	94.74 \pm 0.00	51.04 \pm 0.11	34.63 \pm 0.05	74.18 \pm 0.10
EVA-02 ViT-B/14	96.49 \pm 0.05	99.88 \pm 0.00	94.74 \pm 0.00	72.19 \pm 0.08	63.53 \pm 0.34	97.13 \pm 0.01
OpenAI ViT-B/16	95.50 \pm 0.09	99.79 \pm 0.00	94.74 \pm 0.00	70.85 \pm 0.49	72.10 \pm 0.65	96.44 \pm 0.03
DINO ViT-B/16	98.58\pm0.04	99.94\pm0.00	94.76\pm0.01	78.82\pm0.05	73.80 \pm 0.43	98.45 \pm 0.06
DINOv2 ViT-B/14	97.80 \pm 0.13	99.93 \pm 0.00	94.74 \pm 0.00	76.73 \pm 0.04	83.20\pm0.16	99.11\pm0.02
Results from Zhang et al. (2024) for models pre-trained on medical data						
BiomedGPT	98.7	-	94.9	-	92.9	-
BiomedCLIP	97.9	-	93.0	-	85.6	-
MedSAM	97.2	-	83.8	-	89.1	-

Table 5: Results of foundation models on OrganAMNIST, OrganCMNIST, and OrganSMNIST.

Methods	OrganAMNIST		OrganCMNIST		OrganSMNIST	
	ACC	AUC	ACC	AUC	ACC	AUC
END-TO-END						
VGG16	96.02 \pm 0.44	99.87 \pm 0.03	93.41 \pm 1.38	99.54 \pm 0.20	81.86 \pm 0.74	97.24 \pm 0.38
DenseNet-121	97.52 \pm 0.25	99.93 \pm 0.02	95.42 \pm 0.09	99.80 \pm 0.02	85.28 \pm 0.27	98.05 \pm 0.06
ResNet-18	96.66 \pm 0.12	99.85 \pm 0.06	94.90 \pm 0.71	99.76 \pm 0.04	84.81 \pm 0.28	97.52 \pm 0.01
EfficientNet-B4	97.17 \pm 0.09	99.83 \pm 0.03	95.37 \pm 0.26	99.79 \pm 0.03	84.32 \pm 0.65	98.17 \pm 0.12
ViT-B/16	97.89\pm0.25	99.96\pm0.01	95.89 \pm 0.43	99.88 \pm 0.01	85.42 \pm 0.58	98.33 \pm 0.05
CLIP ViT-B/16	97.67 \pm 0.37	99.93 \pm 0.01	96.09 \pm 0.08	99.89\pm0.00	85.65\pm0.13	98.26 \pm 0.07
SAM-C ViT-B/16	97.76 \pm 0.17	99.91 \pm 0.01	96.15 \pm 0.08	99.72 \pm 0.07	84.69 \pm 0.20	96.96 \pm 0.40
SAM ViT-B/16	95.90 \pm 0.29	99.63 \pm 0.15	94.69 \pm 0.09	99.01 \pm 0.12	82.41 \pm 0.10	97.01 \pm 0.27
EVA-02 ViT-B/14	97.72 \pm 0.35	99.34 \pm 0.16	95.67 \pm 0.25	98.37 \pm 0.09	85.25 \pm 0.40	91.42 \pm 1.46
OpenAI ViT-B/16	97.25 \pm 0.04	99.90 \pm 0.01	95.78 \pm 0.29	99.81 \pm 0.01	84.71 \pm 0.53	98.01 \pm 0.18
DINO ViT-B/16	97.59 \pm 0.16	99.91 \pm 0.02	95.10 \pm 0.14	99.83 \pm 0.01	83.15 \pm 0.56	98.05 \pm 0.16
DINOv2 ViT-B/14	97.81 \pm 0.09	99.91 \pm 0.01	96.16\pm0.20	99.88 \pm 0.01	84.46 \pm 0.82	98.41\pm0.07
LINEAR PROBING						
VGG16	91.56 \pm 0.07	99.54 \pm 0.00	85.83 \pm 0.09	98.85 \pm 0.00	73.07 \pm 0.08	96.58 \pm 0.01
DenseNet-121	91.53 \pm 0.11	99.52 \pm 0.01	86.45 \pm 0.02	99.05 \pm 0.01	74.86 \pm 0.20	97.01 \pm 0.02
ResNet-18	87.05 \pm 0.20	98.95 \pm 0.01	82.57 \pm 0.22	98.29 \pm 0.02	69.79 \pm 0.16	95.95 \pm 0.02
EfficientNet-B4	87.51 \pm 0.09	98.99 \pm 0.01	82.26 \pm 0.06	98.46 \pm 0.01	69.32 \pm 0.16	95.77 \pm 0.03
ViT-B/16	93.02 \pm 0.03	99.65 \pm 0.00	88.42 \pm 0.05	99.22 \pm 0.01	77.66 \pm 0.12	97.59 \pm 0.01
CLIP ViT-B/16	90.87 \pm 0.09	99.44 \pm 0.01	85.14 \pm 0.12	98.84 \pm 0.00	74.94 \pm 0.26	96.94 \pm 0.03
SAM-C ViT-B/16	93.58 \pm 0.05	99.68 \pm 0.00	89.67 \pm 0.07	99.37 \pm 0.00	78.93 \pm 0.07	97.84 \pm 0.00
SAM ViT-B/16	68.69 \pm 0.07	94.76 \pm 0.01	68.29 \pm 0.07	94.25 \pm 0.01	54.81 \pm 0.01	90.59 \pm 0.01
EVA-02 ViT-B/14	91.51 \pm 0.03	99.55 \pm 0.00	86.90 \pm 0.26	99.00 \pm 0.01	77.32 \pm 0.16	97.49 \pm 0.03
OpenAI ViT-B/16	88.40 \pm 0.07	99.17 \pm 0.00	82.66 \pm 0.03	98.48 \pm 0.00	74.19 \pm 0.38	96.82 \pm 0.06
DINO ViT-B/16	94.68\pm0.06	99.79\pm0.01	91.63\pm0.21	99.56\pm0.00	79.42\pm0.07	97.85\pm0.00
DINOv2 ViT-B/14	91.99 \pm 0.11	99.54 \pm 0.01	87.03 \pm 0.15	98.96 \pm 0.01	76.66 \pm 0.16	97.38 \pm 0.01
Results from Zhang et al. (2024) for models pre-trained on medical data						
BiomedGPT	-	-	91.0	-	-	-
BiomedCLIP	-	-	92.5	-	-	-
MedSAM	-	-	90.6	-	-	-

Table 6: Results of foundation models on PathMNIST, RetinaMNIST, and TissueMNIST.

Methods	PathMNIST		RetinaMNIST		TissueMNIST	
	ACC	AUC	ACC	AUC	ACC	AUC
END-TO-END						
VGG16	95.22 \pm 0.55	99.58 \pm 0.13	66.00 \pm 1.59	85.17 \pm 1.49	71.08 \pm 0.46	94.17 \pm 0.05
DenseNet-121	95.06 \pm 1.00	99.72 \pm 0.03	65.17 \pm 2.82	82.10 \pm 0.84	73.84 \pm 0.34	95.22 \pm 0.07
ResNet-18	94.40 \pm 1.41	99.64 \pm 0.16	62.33 \pm 1.05	80.55 \pm 0.34	71.70 \pm 0.37	94.44 \pm 0.06
EfficientNet-B4	94.32 \pm 0.90	99.61 \pm 0.08	63.58 \pm 0.96	83.42 \pm 0.69	75.56 \pm 0.44	95.69 \pm 0.10
ViT-B/16	96.69 \pm 0.52	99.72 \pm 0.02	63.17 \pm 0.51	83.11 \pm 0.77	75.92 \pm 0.38	95.85\pm0.11
CLIP ViT-B/16	96.50 \pm 0.24	99.75 \pm 0.01	66.08 \pm 1.64	85.79 \pm 1.18	75.05 \pm 0.27	95.47 \pm 0.10
SAM-C ViT-B/16	96.99\pm0.25	99.45 \pm 0.11	65.08 \pm 1.48	80.36 \pm 2.33	74.92 \pm 0.15	95.41 \pm 0.08
SAM ViT-B/16	95.97 \pm 0.43	98.66 \pm 0.66	60.17 \pm 1.05	76.07 \pm 1.93	70.76 \pm 0.70	94.10 \pm 0.30
EVA-02 ViT-B/14	96.80 \pm 0.43	98.64 \pm 0.25	64.92 \pm 0.66	78.92 \pm 2.48	75.92\pm0.28	92.91 \pm 0.24
OpenAI ViT-B/16	95.68 \pm 0.72	99.65 \pm 0.10	68.67 \pm 0.72	84.91 \pm 1.33	74.96 \pm 0.21	95.52 \pm 0.09
DINO ViT-B/16	96.97 \pm 0.33	99.75\pm0.01	63.75 \pm 1.62	82.60 \pm 0.79	74.69 \pm 0.34	95.43 \pm 0.11
DINOv2 ViT-B/14	95.55 \pm 1.14	99.59 \pm 0.19	70.50\pm1.24	89.26\pm0.63	73.88 \pm 0.61	95.29 \pm 0.13
LINEAR PROBING						
VGG16	88.23 \pm 0.08	98.81 \pm 0.01	59.83 \pm 1.53	83.96 \pm 0.49	57.21 \pm 0.04	87.30 \pm 0.01
DenseNet-121	93.30 \pm 0.22	99.35 \pm 0.03	62.83 \pm 0.62	83.34 \pm 0.44	55.96 \pm 0.04	86.25 \pm 0.01
ResNet-18	90.58 \pm 0.34	99.22 \pm 0.01	61.08 \pm 0.62	82.26 \pm 0.16	52.20 \pm 0.07	83.99 \pm 0.02
EfficientNet-B4	88.94 \pm 0.25	98.77 \pm 0.09	57.33 \pm 1.39	77.33 \pm 1.09	49.31 \pm 0.08	80.82 \pm 0.09
ViT-B/16	93.68 \pm 0.17	99.64 \pm 0.01	59.92 \pm 0.77	83.89 \pm 0.18	62.24 \pm 0.01	90.08 \pm 0.02
CLIP ViT-B/16	91.30 \pm 0.16	99.24 \pm 0.02	62.00 \pm 0.61	85.85 \pm 0.10	60.34 \pm 0.09	89.07 \pm 0.01
SAM-C ViT-B/16	93.74 \pm 0.06	99.51 \pm 0.01	62.92 \pm 0.47	85.69 \pm 0.05	59.32 \pm 0.03	88.59 \pm 0.01
SAM ViT-B/16	66.06 \pm 0.09	93.42 \pm 0.01	43.50 \pm 0.00	55.26 \pm 3.93	43.98 \pm 0.00	72.42 \pm 0.02
EVA-02 ViT-B/14	93.53 \pm 0.07	99.60 \pm 0.00	66.00 \pm 0.20	86.11 \pm 0.01	59.72 \pm 0.05	88.75 \pm 0.01
OpenAI ViT-B/16	93.27 \pm 0.05	99.52 \pm 0.01	62.75 \pm 0.54	84.10 \pm 0.04	57.94 \pm 0.04	87.62 \pm 0.02
DINO ViT-B/16	96.20\pm0.09	99.78\pm0.01	63.25 \pm 1.67	85.27 \pm 0.10	62.78\pm0.08	90.33\pm0.01
DINOv2 ViT-B/14	93.82 \pm 0.07	99.49 \pm 0.00	69.08\pm0.66	88.12\pm0.47	61.98 \pm 0.06	89.92 \pm 0.01
Results from Zhang et al. (2024) for models pre-trained on medical data						
BiomedGPT	95.8	-	-	-	-	-
BiomedCLIP	91.0	-	-	-	-	-
MedSAM	84.2	-	-	-	-	-

Appendix D. Results of Foundation Models on DermaMNIST with Different Image sizes

Table 7: Results of foundation models on DermaMNIST of different image sizes using zero-padding to resize the original images into a resolution of 224×224 .

Methods	28×28		64×64		128×128	
	ACC	AUC	ACC	AUC	ACC	AUC
END-TO-END						
VGG16	79.62 \pm 0.94	91.98 \pm 0.46	84.26\pm0.58	94.93 \pm 0.45	86.80 \pm 0.21	96.96 \pm 0.18
DenseNet-121	76.11 \pm 0.57	87.65 \pm 1.24	81.86 \pm 0.36	93.76 \pm 0.63	85.60 \pm 0.19	95.69 \pm 0.30
ResNet-18	77.71 \pm 0.71	90.87 \pm 0.75	81.16 \pm 1.18	93.34 \pm 1.11	84.22 \pm 0.68	95.26 \pm 0.13
EfficientNet-B4	73.85 \pm 0.56	88.40 \pm 0.75	78.72 \pm 0.82	92.51 \pm 0.75	84.74 \pm 1.63	95.87 \pm 0.47
ViT-B/16	78.77 \pm 0.16	92.82 \pm 0.40	83.52 \pm 0.89	96.13\pm0.27	86.32 \pm 0.24	97.37 \pm 0.07
CLIP ViT-B/16	79.67\pm0.80	92.57 \pm 0.22	82.96 \pm 0.69	95.45 \pm 0.52	86.93 \pm 0.19	97.51 \pm 0.07
SAM-C ViT-B/16	77.37 \pm 0.76	89.25 \pm 0.75	81.00 \pm 1.40	93.48 \pm 0.45	85.07 \pm 0.20	95.30 \pm 0.18
SAM ViT-B/16	73.95 \pm 0.48	79.83 \pm 0.90	75.79 \pm 1.12	84.00 \pm 2.90	78.34 \pm 0.36	87.21 \pm 1.31
EVA-02 ViT-B/14	78.87 \pm 0.72	83.27 \pm 1.32	82.11 \pm 0.35	87.51 \pm 1.17	85.89 \pm 0.25	92.17 \pm 2.00
OpenAI ViT-B/16	78.94 \pm 0.49	92.45 \pm 0.13	83.28 \pm 0.26	95.44 \pm 0.29	87.22 \pm 0.59	97.12 \pm 0.20
DINO ViT-B/16	78.35 \pm 0.11	93.14\pm0.19	81.83 \pm 0.49	95.49 \pm 0.37	85.34 \pm 0.43	97.10 \pm 0.06
DINOv2 ViT-B/14	76.79 \pm 0.72	92.13 \pm 0.54	81.68 \pm 0.76	94.96 \pm 0.67	87.35\pm0.06	97.60\pm0.02
LINEAR PROBING						
VGG16	73.47 \pm 0.18	88.76 \pm 0.07	75.79 \pm 0.27	89.70 \pm 0.08	76.86 \pm 0.07	91.29 \pm 0.02
DenseNet-121	70.27 \pm 0.07	85.13 \pm 1.33	71.80 \pm 0.16	87.33 \pm 0.03	75.98 \pm 0.33	91.34 \pm 0.14
ResNet-18	69.68 \pm 0.19	82.37 \pm 0.19	68.43 \pm 0.15	83.23 \pm 0.04	72.92 \pm 0.24	88.34 \pm 0.03
EfficientNet-B4	68.23 \pm 0.15	81.28 \pm 0.45	70.09 \pm 0.20	84.62 \pm 0.26	72.14 \pm 0.13	86.97 \pm 0.57
ViT-B/16	72.52 \pm 0.14	90.74 \pm 0.17	78.59 \pm 0.30	94.18 \pm 0.04	81.91 \pm 0.22	95.54 \pm 0.03
CLIP ViT-B/16	74.58 \pm 0.24	90.47 \pm 0.16	77.27 \pm 0.19	93.54 \pm 0.05	81.23 \pm 0.22	95.13 \pm 0.02
SAM-C ViT-B/16	73.67 \pm 0.07	90.16 \pm 0.06	78.99 \pm 0.25	94.59 \pm 0.02	80.45 \pm 0.08	95.57 \pm 0.03
SAM ViT-B/16	66.88 \pm 0.00	55.42 \pm 2.35	66.88 \pm 0.00	46.89 \pm 2.67	66.88 \pm 0.00	52.40 \pm 1.05
EVA-02 ViT-B/14	75.48 \pm 0.06	92.40 \pm 0.03	78.89 \pm 0.27	94.28 \pm 0.06	81.68 \pm 0.10	95.31 \pm 0.01
OpenAI ViT-B/16	75.81 \pm 0.11	91.82 \pm 0.05	79.62 \pm 0.10	94.36 \pm 0.02	80.62 \pm 0.02	95.36 \pm 0.01
DINO ViT-B/16	77.07 \pm 0.20	92.52 \pm 0.09	80.83\pm0.16	95.53\pm0.05	82.78\pm0.17	96.42\pm0.05
DINOv2 ViT-B/14	77.37\pm0.25	92.91\pm0.27	79.55 \pm 0.08	94.41 \pm 0.03	81.88 \pm 0.50	95.34 \pm 0.20

Appendix E. Plots of Performance Comparison on DermaMNIST with Different Image Sizes and Image Resizing Strategies

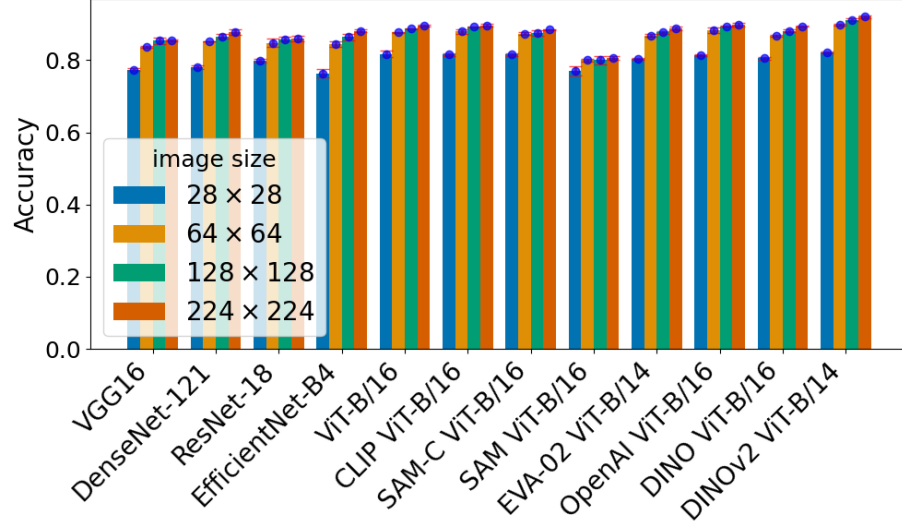


Figure 15: Performance comparison of foundation models on DermaMNIST with different image sizes, when using end-to-end fine-tuning and scaling for image resizing.

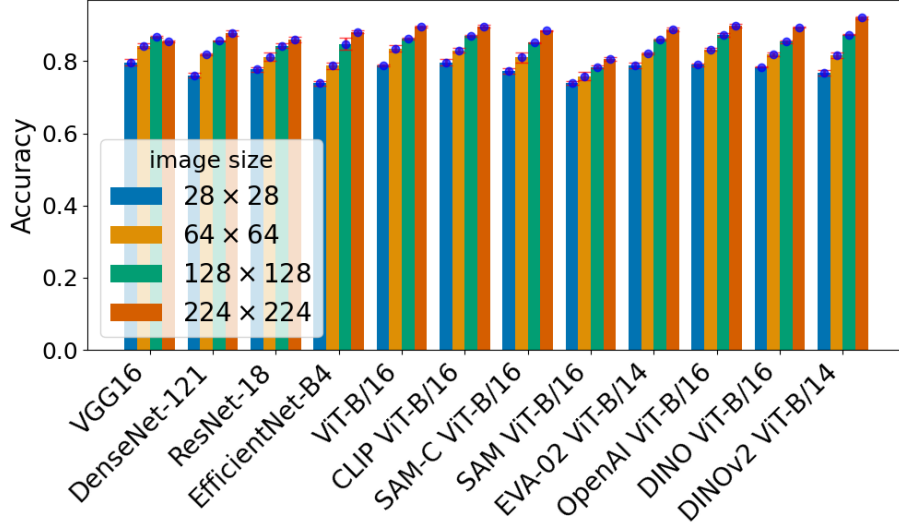


Figure 16: Performance comparison of foundation models on DermaMNIST with different image sizes, when using end-to-end fine-tuning and zero-padding for image re-sizing.

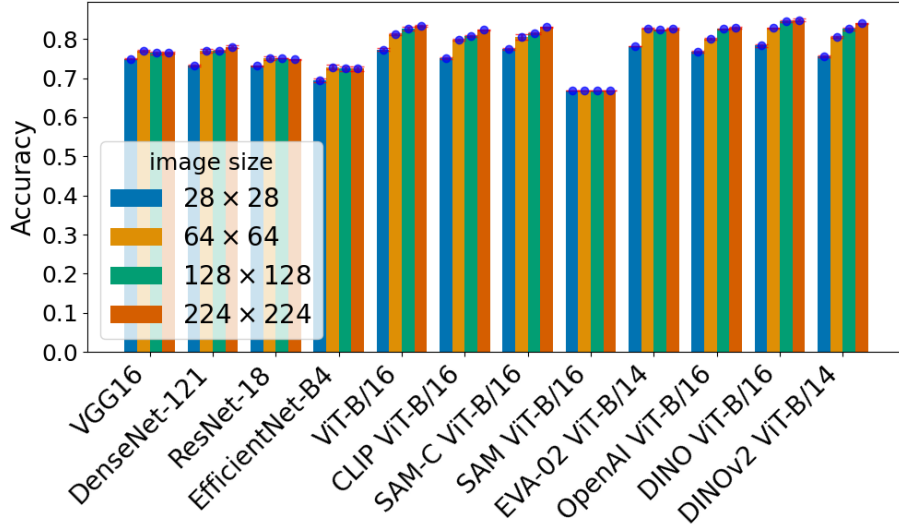


Figure 17: Performance comparison of foundation models on DermaMNIST with different image sizes, when using linear probing and scaling for image re-sizing.

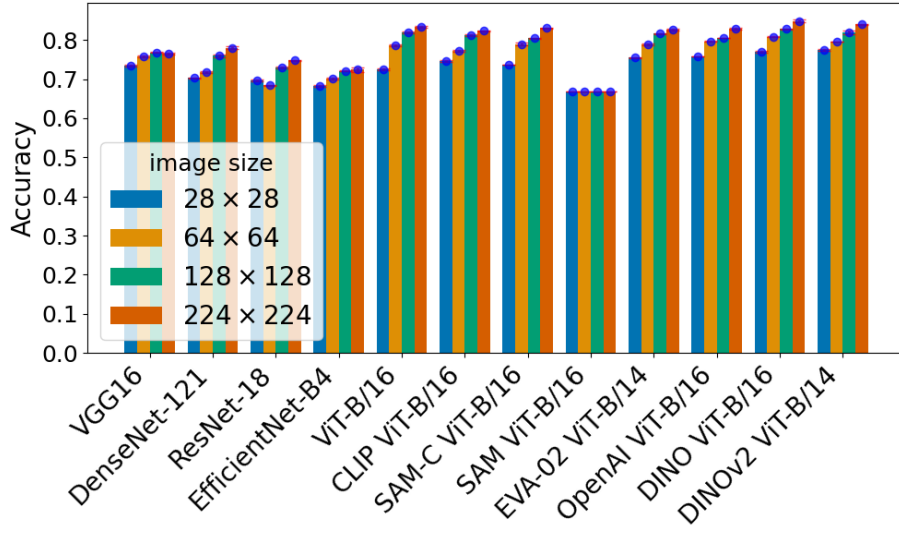


Figure 18: Performance comparison of foundation models on DermaMNIST with different image sizes, when using linear probing and zero-padding for image resizing.

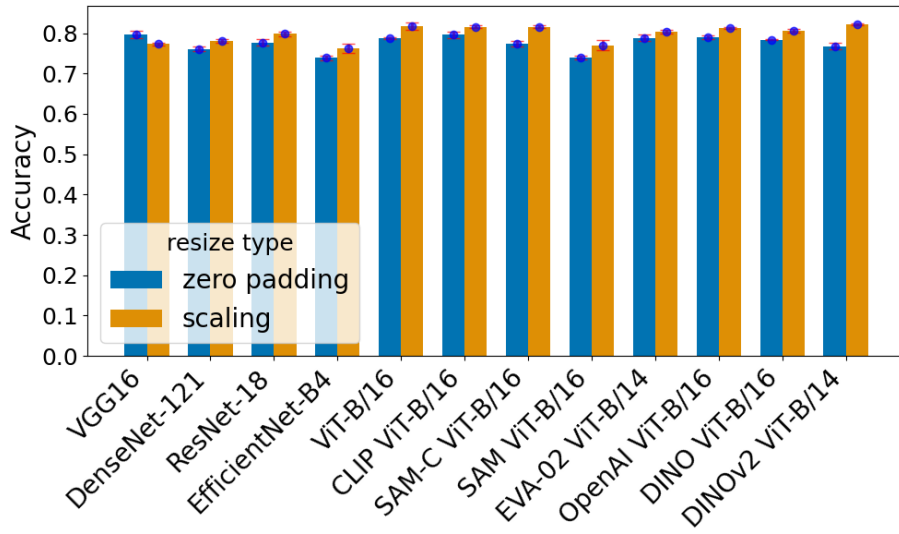


Figure 19: Performance comparison for zero-padding and scaling on DermaMNIST with an image size of 28×28 , when using end-to-end fine-tuning.

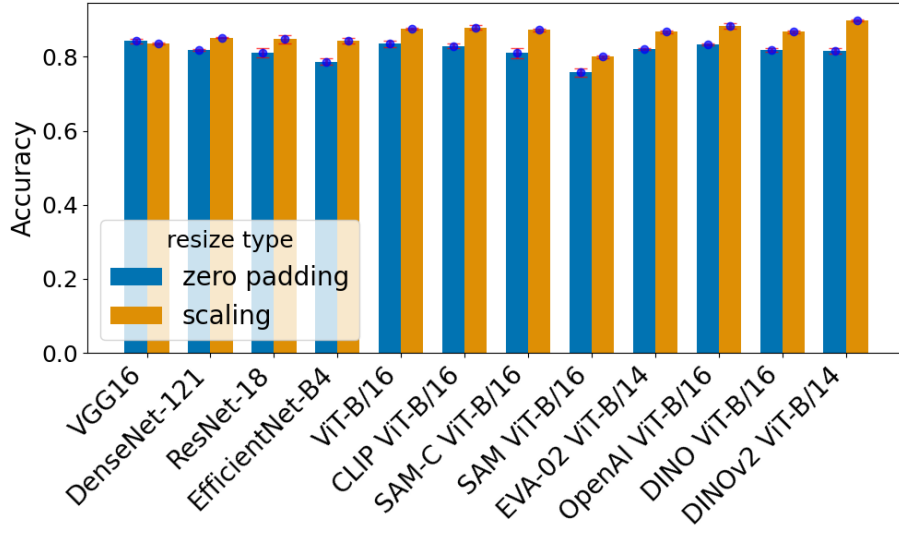


Figure 20: Performance comparison for zero-padding and scaling on DermaMNIST with an image size of 64×64 , when using end-to-end fine-tuning.

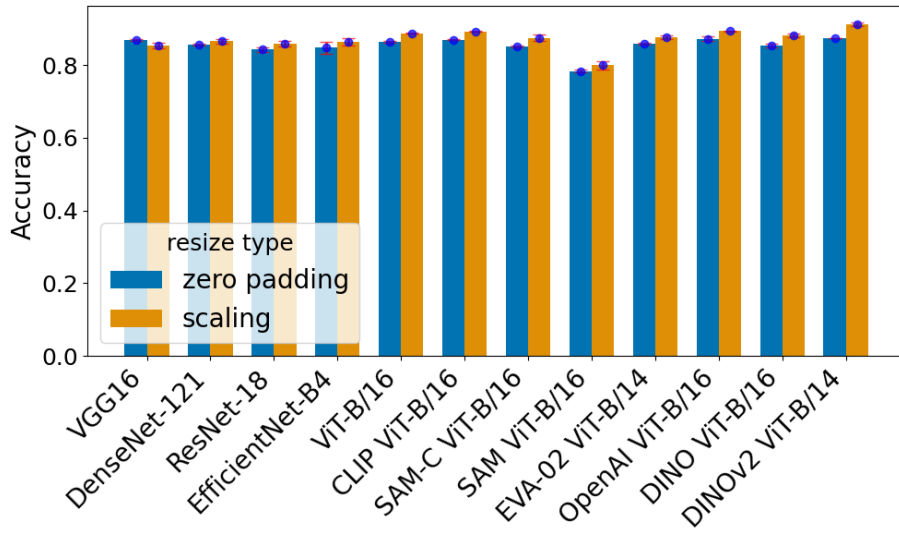


Figure 21: Performance comparison for zero-padding and scaling on DermaMNIST with an image size of 128×128 , when using end-to-end fine-tuning.

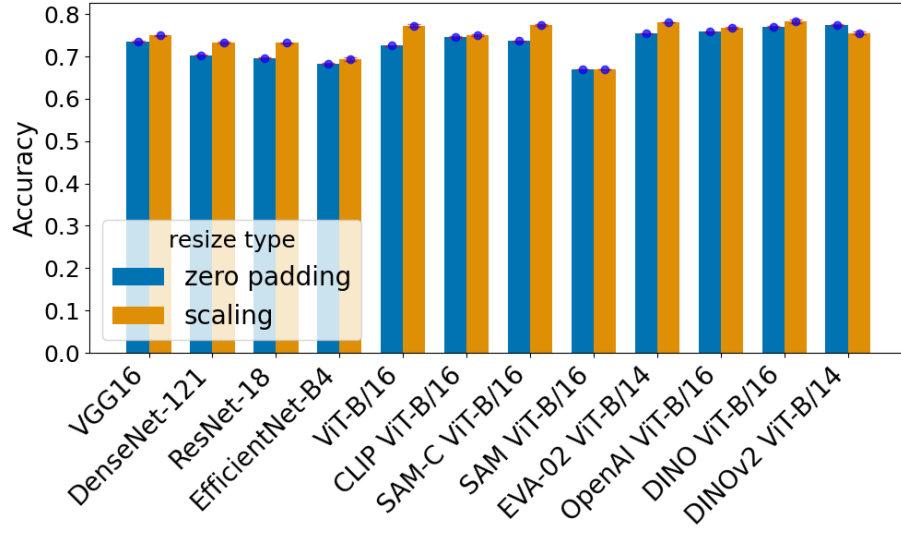


Figure 22: Performance comparison for zero-padding and scaling on DermaMNIST with an image size of 28×28 , when using linear probing.

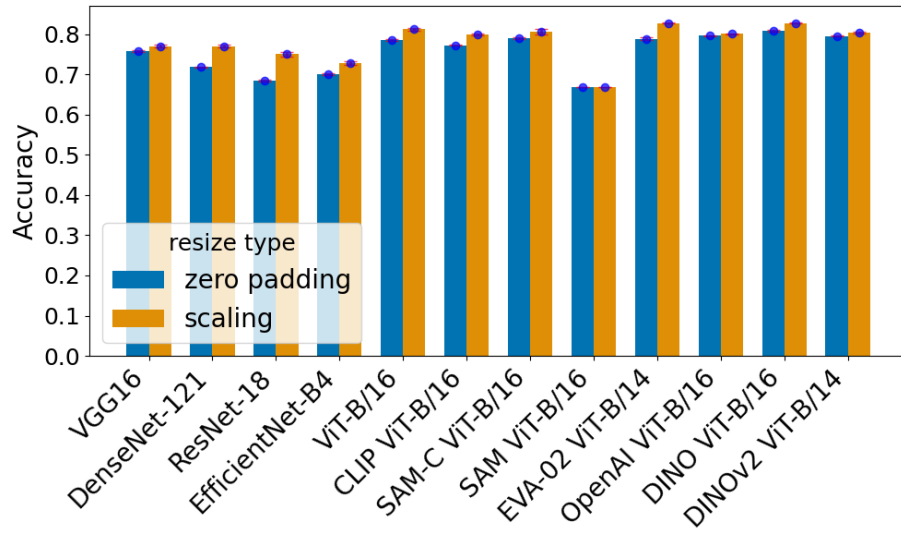


Figure 23: Performance comparison for zero-padding and scaling on DermaMNIST with an image size of 64×64 , when using linear probing.

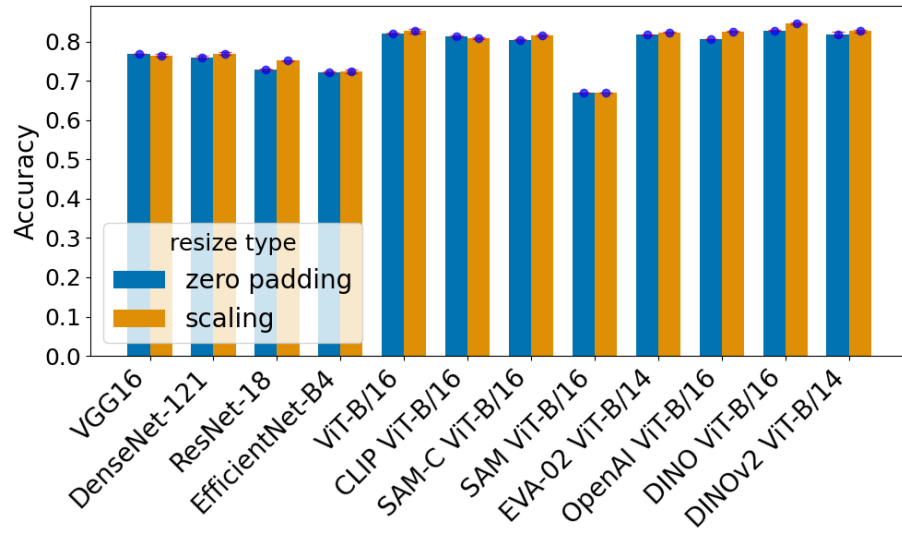


Figure 24: Performance comparison for zero-padding and scaling on DermaMNIST with an image size of 128×128 , when using linear probing.

Appendix F. Plots of Performance Changes with Various Numbers of DermaMNIST Training Data

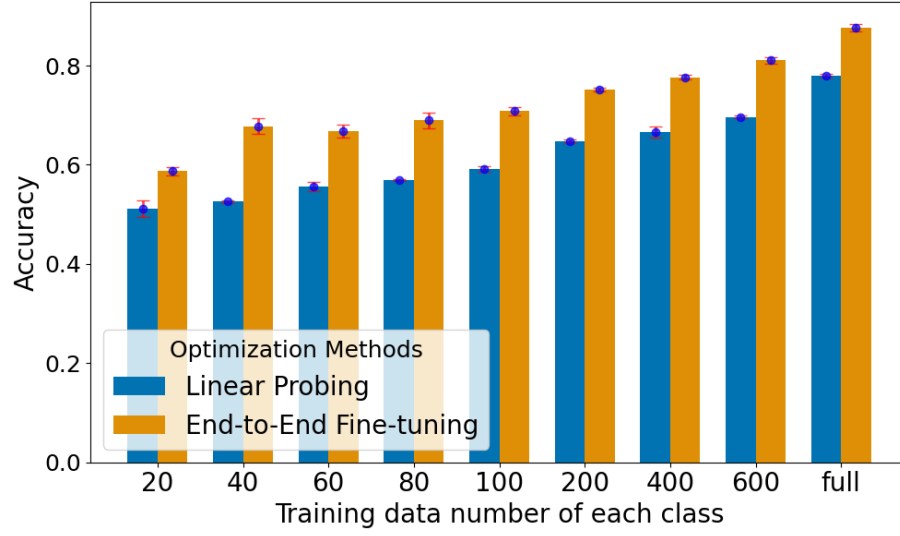


Figure 25: Accuracy of DenseNet-121 on DermaMNIST when training model with a different number of data for each class.

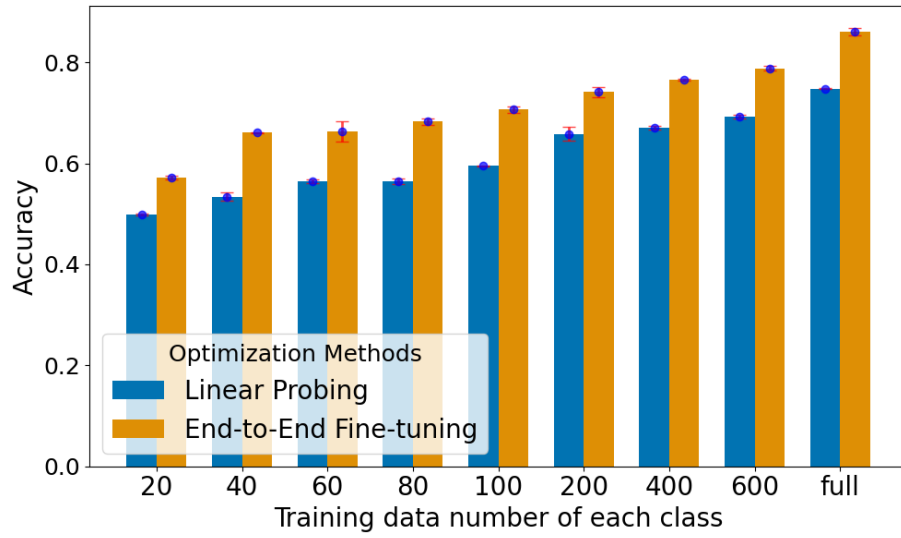


Figure 26: Accuracy of ResNet-18 on DermaMNIST when training model with a different number of data for each class.

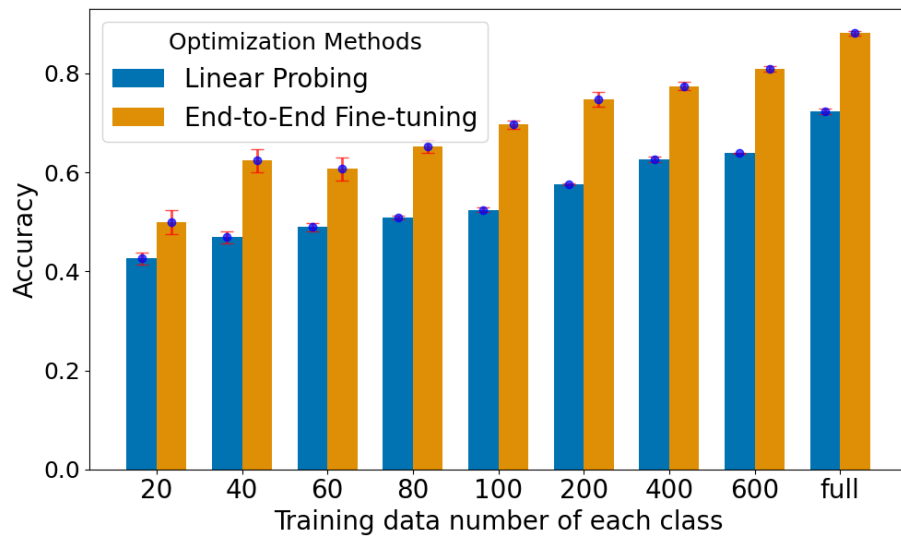


Figure 27: Accuracy of EfficientNet-B4 on DermaMNIST when training model with a different number of data for each class.

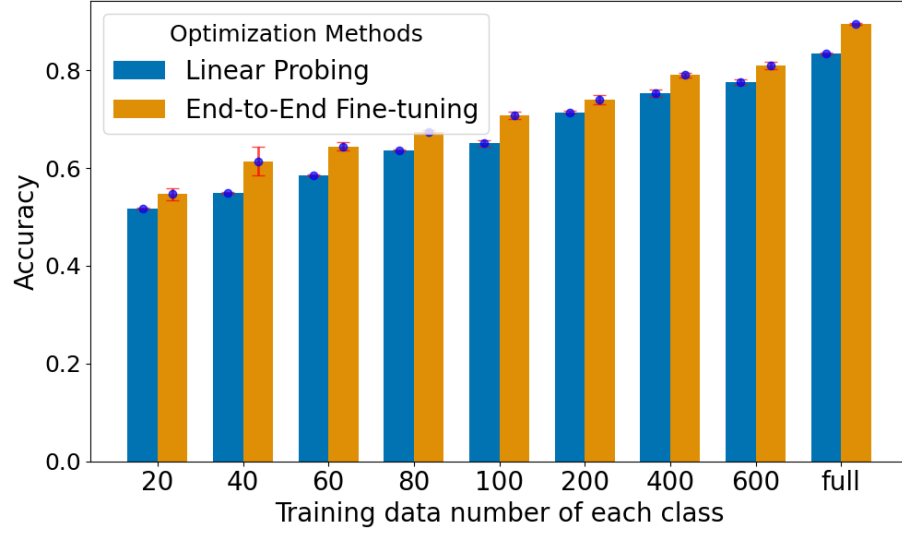


Figure 28: Accuracy of ViT-B/16 on DermaMNIST when training model with a different number of data for each class.

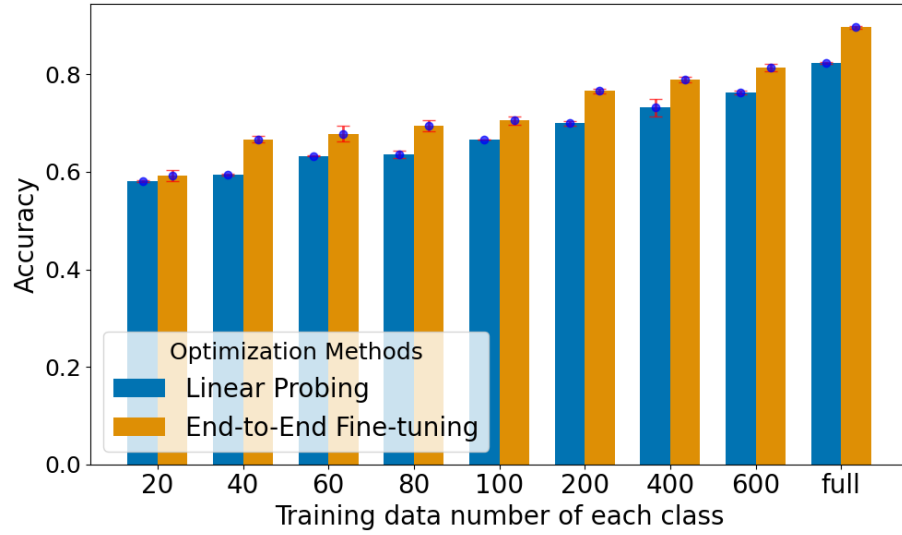


Figure 29: Accuracy of CLIP ViT-B/16 on DermaMNIST when training model with a different number of data for each class.

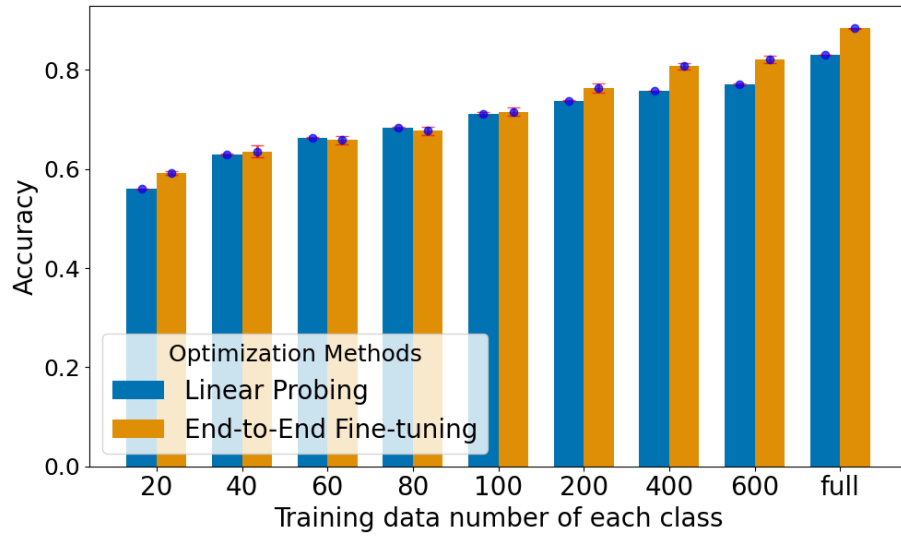


Figure 30: Accuracy of SAM-C ViT-B/16 on DermaMNIST when training model with a different number of data for each class.

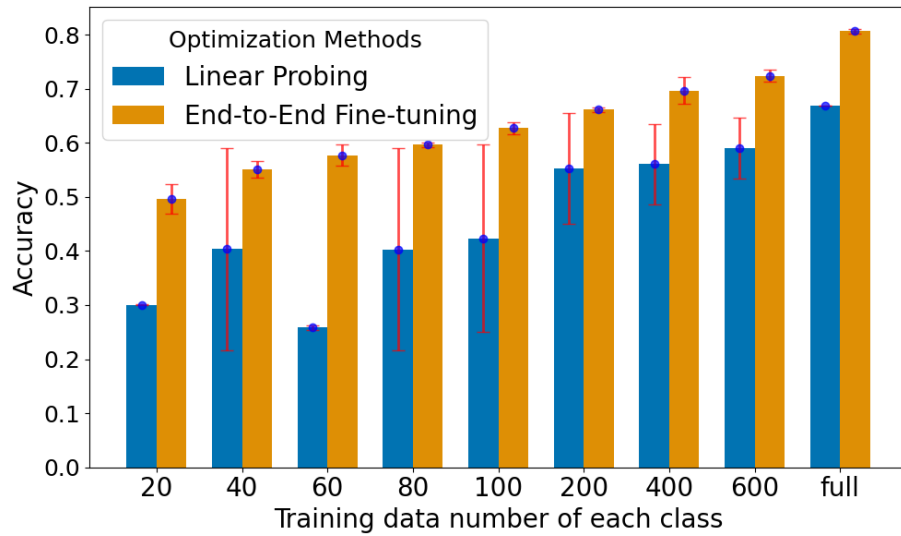


Figure 31: Accuracy of SAM ViT-B/16 on DermaMNIST when training model with a different number of data for each class.

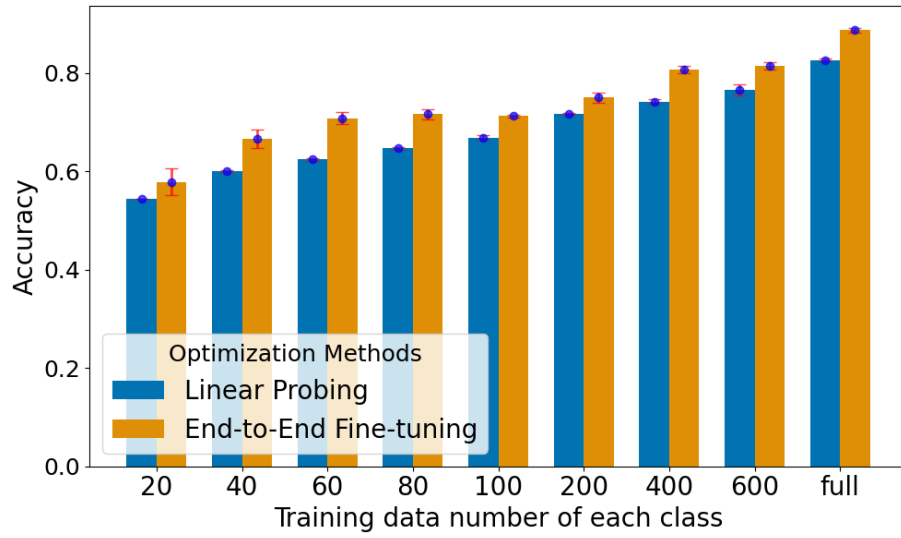


Figure 32: Accuracy of EVA-02 ViT-B/14 on DermaMNIST when training model with a different number of data for each class.

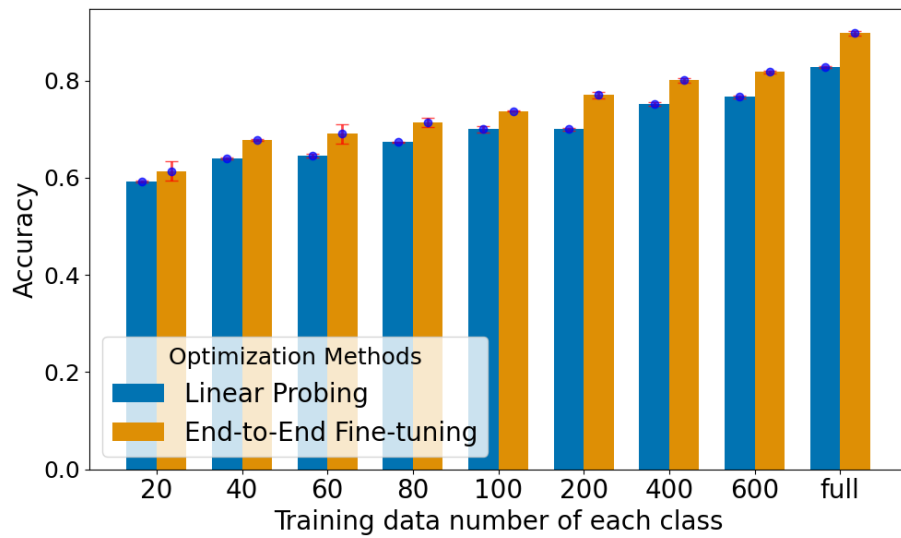


Figure 33: Accuracy of DINO OpenAI ViT-B/16 on DermaMNIST when training model with a different number of data for each class.

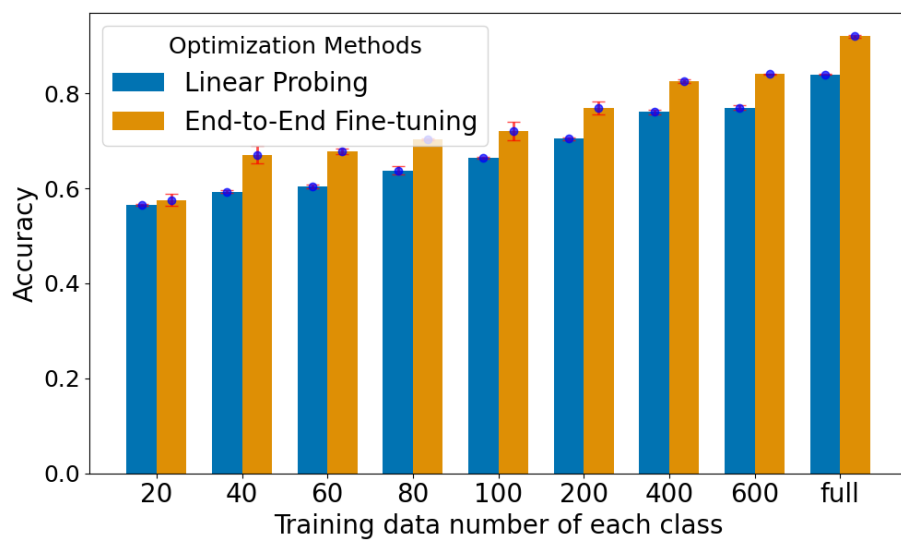


Figure 34: Accuracy of DINOv2 ViT-B/14 on DermaMNIST when training model with a different number of data for each class.

